Electronics system integration and characterization of electronic skin for prosthetic applications.

by

Muhammad Awais

A Dissertation Submitted to the
Graduate School of Sciences and Engineering
in Partial Fulfillment of the Requirements for
the Degree of

Master of Science

in

Biomedical Science and Engineering

January 12, 2024

Electronics system integration and characterization of electronic skin for prosthetic applications.

Koç University

Graduate School of Sciences and Engineering

This is to certify that I have examined this copy of a master's thesis by

Muhammad Awais

and have found that it is complete and satisfactory in all respects,
and that any and all revisions required by the final
examining committee have been made.

Committee Members:

_____

Assist. Prof. Levent Beker (Advisor)

_____

Assist. Prof. Beren Semiz

_____

Assist. Prof. Emin Istif

Date: _____

I dedicate this thesis to the unwavering support and boundless love of my parents, whose encouragement and sacrifices have been the driving force behind my academic journey. Your belief in my abilities has been a constant source of inspiration. I hope this achievement will fulfill the dream you envisioned for me. "My Lord, have mercy upon them as they brought me up [when I was] small."

ABSTRACT

Electronics system integration and characterization of electronic skin for prosthetic applications.

Muhammad Awais

Master of Science in Biomedical Science and Engineering

January 12, 2024

Upper limb amputation significantly disrupts tactile perception, having a crucial impact on daily activities. For attaining a prosthetic device that closely mimics natural functioning, it is crucial to provide users with enhanced sensory experiences during interactions with objects. Through sensory feedback, the ideal upper limb prosthesis must provide real-time mirroring of the user's natural experiences. Current prostheses face challenges in delivering substantial tactile feedback due to their limited sensory capabilities. Here, inspired by the sensory characteristics of the skin, we describe a micro-fabricated and multiplexed electronic skin that is combined with a suite of actuators for sensory feedback capabilities, and employed for upper limb amputation. The set of piezoelectric-capacitive sensors can identify static pressure, temperature, vibration, and texture, while the incorporated actuators offer instantaneous feedback through skin stimulation. The fabricated sensor array has a flexible structure and a compact design of two pixels inside a 1 cm^2 footprint. This array of sensors is capable of detecting a wide range of pressure (0.5-10 kPa), temperature (22-60 °C), vibration (35-100 Hz), and texture (2.5-45 Hz) which are the most important tactile sensations of the human skin. The electronic skin is affixed to a prosthetic finger, while the actuators are positioned on the wrists of the human volunteers. Human participants participated in feasibility tests of the system, and its performance was quantitatively evaluated using statistical methods. The incorporation of multiplexed sensors and actuators introduces novel prospects for delivering improved tactile feedback and enhancing the quality of life for individuals with upper limb amputation.

ÖZETÇE

Yüksek Lisans Tez Başlığı

Muhammad Awais

Biyomedikal Bilim ve Mühendislik, Yüksek Lisans

12 Ocak 2024

Üst ekstremite amputasyonu, dokunma algısını önemli ölçüde bozar ve günlük aktiviteler üzerinde etkili bir rol oynar. Doğal işlevselliği yakından taklit eden protez bir cihaz elde etmek için, kullanıcılara nesnelerle etkileşim sırasında geliştirilmiş duyusal deneyimler sunmak kritiktir. Gerçek zamanlı olarak kullanıcının doğal deneyimlerini yansıtmak için, ideal üst ekstremite protezi, güçlendirilmiş duyusal geribildirim sağlamalıdır. Mevcut protezler, sınırlı duyusal yetenekleri nedeniyle önemli dokunsal geribildirim sunma konusunda zorluklarla karşılaşmaktadır. Burada, cildin duyusal özelliklerinden esinlenerek, üst ekstremite amputasyonu için kullanılan mikro fabrikasyon ve multiplex elektronik ciltten bahsediyoruz. Duyusal geribildirim yetenekleri için bir dizi aktuatörle birleştirilmiş olan bu elektronik cilt, kullanıcıların doğal deneyimlerini gerçek zamanlı olarak yansıtmak üzere tasarlanmıştır. Piezoelektrik-kapasitif sensörler kümesi, statik basınç, sıcaklık, titreşim ve doku tanımlayabilirken, içerilen aktuatörler cilt stimülasyonu aracılığıyla anında geri bildirim sunar. Üretilen sensör dizisi, 1 cm² bir alan içinde iki pikselin esnek bir yapısı ve kompakt bir tasarımına sahiptir. Bu sensör dizisi, insan cildinin en önemli dokunsal duyumları olan geniş bir basınç (0.5-10 kPa), sıcaklık (22-60 °C), titreşim (35-100 Hz) ve doku (2.5-45 Hz) aralığını algılayabilir. Elektronik cilt, bir protez parmağına yerleştirilmişken, aktuatörler insan gönüllülerinin bileklerine yerleştirilmiştir. İnsan katılımcıları, sistemin olasılık testlerine katıldı ve performansı istatistiksel yöntemler kullanılarak nicel olarak değerlendirildi. Multiplex sensörlerin ve aktuatörlerin entegrasyonu, geliştirilmiş dokunsal geribildirim sağlama ve üst ekstremite amputasyonu olan bireylerin yaşam kalitesini artırma konusunda yeni olanaklar sunmaktadır.

AKNOWLEDGEMENTS

First and foremost, I extend my heartfelt gratitude to Dr. Levent Beker for giving me the opportunity to contribute to the Bio-integrated Microdevices Laboratory. His role as my advisor, along with his unwavering support, guidance, and patience, has been invaluable to the completion of this master's thesis. Dr. Beker's visionary mindset and vast experience are shaping influences that will continue to guide me in my career. I am truly fortunate to have had his mentorship, and I look forward to applying the insights gained in future pursuits.

I would also like to thank Dr. Beren Semiz and Dr. Emin Istif for their crucial roles as committee members in evaluating my thesis. Their valuable insights and thoughtful comments have greatly enriched the quality of my work, and I am grateful for their constructive contributions to this academic endeavor.
I would like to especially thank Professor Cagtay Basdoag and Professor Kemal Turker for their collaboration, guidance, and sharing their experiences with us. I am also grateful to my collaborators whose support was instrumental in the success of this project.

I would like to express my sincere gratitude to my friends, Ritu Das, Basit Ali, Mohsin Ali, Nasir Khan, Tufail Ahmad, Hammad Ur Rehman, Hafiz Fareed Ahmad, and Abdullah Nadeem, for their unwavering friendship and support throughout this academic journey. I am fortunate to have such a supportive circle, and their presence has added immeasurable value to both my personal and academic experiences.

Special thanks to my cricket community and cards-playing friends for providing a refreshing outlet during the intensity of academic pursuits. Your friendship and shared moments of relaxation have been a vital source of balance and joy.

Last but not least, my deepest gratitude goes to my family, especially my parents, whose unwavering support has been the foundation of my academic endeavors. Their encouragement, understanding, and sacrifices have played a pivotal role in my success, and I am profoundly thankful for their love and guidance throughout this journey.

TABLE OF CONTENTS

LIST OF TABLES

LIST OF FIGURES

ABBREVIATIONS

E-skin	Electronic skin
PVDF-TrFE	Poly vinylidene fluoride -trifluoro ethylene
PCB	Printed circuit board
FFT	Fast Fourier Transform
SEM	Scanning electron microscopy

Chapter 1:
INTRODUCTION

1.1 Background

The rising global demand for limb prostheses is driven by an aging population, increased accidents, health-related amputations, a surge in diabetic cases, and complications from vascular diseases (Raichle et al., 2008). While prosthetic limbs have evolved to restore motor functions, there remains a significant challenge in replicating the intricate sense of touch human skin offers. It is projected that by 2050, approximately 3.6 million individuals in the United States will rely on prosthetic limbs as assistive devices (Ziegler-Graham et al., 2008). Human skin receptors detect tactile inputs such as pressure, temperature, vibration, and texture (Jones et al., 2006). Therefore, a continuous sensing mechanism is required to closely emulate human skin's sensitivity and responsiveness to various stimuli. With the ongoing advancements in electronic skin (e-skin) technology, the restoration of human tactile sensing in prosthetic hands becomes feasible. E-skin holds promise in applications such as haptic feedback (S. Chen et al., 2023; Jung et al., 2022a; D. Li et al., 2021, 2022; Yin et al., 2021), prosthetics (Chortos et al., 2016; D'Anna et al., 2019; Kwak et al., 2020; P. Li et al., 2020; Liang et al., 2019; Petrini et al., 2019), intelligent robotics (Boutry et al., 2018; F. Liu et al., 2022; Y. Liu et al., 2022; Shih et al., 2020; Thuruthel et al., 2019; Yao et al., 2020), and human-machine interfaces (Yu et al., 2020; M. Zhu et al., 2020). Yet, an ideal e-skin system must possess multifunctional capabilities to simultaneously detect various types of stimuli (Bae et al., 2018; Cai et al., 2021; Qiu et al., 2020; S. Zhao et al., 2017) while also fostering a sense of ownership or embodiment of the prosthetic limb (Farina et al., 2014).

1.2 Literature review

E-skin typically consists of flexible and stretchable materials capable of detecting physical parameters similar to the human sense of touch. While the implementation of sensations such as pressure (D. Li et al., 2022), temperature and pressure (Kwak et al., 2020), vibration, and texture (Bensmaïa et al., 2003; Rostamian et al., 2022) has made

gradual progress, the full multifunctional capacity of the human tactile system remains underestimated. Consequently, multifunctional e-skins, composed of stretchable matrix networks, have been proposed for pressure, temperature, and material sensing (Y. Chen et al., 2022; Fastier-Wooller et al., 2021; Pang et al., 2022; Wang et al., 2020). Various phenomena such as piezoelectricity, piezo resistivity, and triboelectricity have been harnessed in these e-skins to enable material discrimination and texture recognition (H. Chen et al., 2017; Cho et al., 2022; Lee et al., 2021; P. Zhu et al., 2020). The combination of capacitive and piezoelectric effects in e-skins enabled the detection of position, dynamic force, proximity, and humidity while achieving a much simpler structure (Dai et al., 2021). In addition, integrating diverse units through a well-considered combination of functional and structural design has led to the development of an e-skin with multifunctional capabilities for pressure, wind flow, and material recognition based on thermosensation (S. Zhao et al., 2017).

On the other hand, e-skin has the potential to empower robots to engage with the world in a more intuitive, safe, and efficient manner. Hence, the integration of multifunctional sensing e-skin into robots, equipped with sensing capabilities for contact force, position, temperature, and proximity, improved the overall human-robot interaction (G. Li et al., 2022). However, the integration of these skins onto prosthetic or robotic hands necessitates specific designs, a challenge addressed through the fabrication of 3D-shaped e-skins (Xiong et al., 2022). Even though individual sensors have been developed for e-skin applications, it is critical to provide a solution or design that is capable of a simple fabrication process, and multiplexed sensing capabilities with a potential for miniaturization to increase pixel density. Moreover, there has been limited research done on combining the multiplexed sensors with the actuators to achieve haptic feedback.

1.3 Our proposed system

To tackle the above-mentioned issues, we propose a novel microfabricated e-skin featuring miniaturized arrays of sensors capable of detecting static pressure, temperature, vibration, and texture. The single piezoelectric layer microfabrication, and the in-plane and double plate type electrode designs enable capacitive and piezoelectric sensing. The signals of the sensors are transmitted to our standalone miniaturized electronics. Since,

our e-skin is specifically designed for applications in upper limb amputations, a test protocol was prepared to understand e-skin performance under various daily activities. Additionally, a set of four actuators was positioned at the wrist to convey corresponding sensations in real time.

1.3.1 Actuators algorithms

We utilized four actuators each for its corresponding sensor; for the pressure sensor, we used a servo motor as a pressure actuator, for the temperature sensor, we used the Peltier module as an actuator. Moreover, for the vibration sensor and texture sensor, we used a coin cell vibration motor as an actuator. We define a range of capacitance and when the value of capacitance increases from the initial value with applied external pressure, the arm of the servo motor rotates to a certain degree. The higher the applied pressure, the higher the degree of rotation. Since the rotating arm of the motor will be pressing the skin of the subject, higher rotation means higher applied pressure on the skin.

We defined 4 ranges of temperature between 30 ℃ and 50 ℃ each with 5 ℃. The actuator gives stimulation only once in every range when the temperature is rising. The higher the temperature range the higher the amplitude of stimulation. There is no stimulation during the falling temperature ranges. The vibration actuation is modality modality-matched feedback mechanism. The algorithm first takes the FFT of the input signal and finds the fundamental frequency at which the object is vibrating. It then vibrates the vibration motor at the same frequency as the input signal. For vibration actuation, both the motors are vibrating simultaneously. We are using vibration motors for both vibration and texture actuation. To distinguish vibration sensation from texture, we are using two vibration motors. For the texture feedback actuation, we vibrate the two motors with a certain delay and that time delay corresponds to the roughness of the surface.

Through experiments, we demonstrate the broad sensing range of our e-skin system, enabling the simultaneous detection of multiple stimuli and feedback mechanisms through actuators. Moreover, our e-skin system was successfully validated in vivo in human trials. The proposed system could have various applications in prosthetics, wearable health monitoring, and human-robot interaction.

Chapter 2:
RESULTS AND DISCUSSION

2.1 The overall e-skin system

The multiplexed, piezoelectric-capacitive-based e-skin system developed in this work transmits the static pressure, temperature, vibration, and texture sensations picked up by the sensors to a group of actuators to provide real-time feedback. Figure 1A illustrates the concept of the e-skin system implemented on a hand prosthesis for the tactile information collection, transmission, and generation of artificial sensation on the human body. Once the tactile signals are received by the sensors, the corresponding actuators are triggered to replicate the production of the sensations to the skin. The exploded view consists of different layers of flexible materials that are used for the fabrication of the single-pixel array of the sensor (right panel of Figure 2.1A). The temperature and static pressure sensors produce a capacitance variation in response to external temperature and static pressure stimuli, respectively (right panel of Figure 2.1B). Likewise, the vibration and texture sensor generate a potential difference due to the piezoelectric effect when subjected to external vibration and texture stimuli, respectively (left panel of Figure 2.1B). The e-skin system can be mounted on the amputated arm with a sensor array attached to the finger of the prosthetic hand to collect data when the finger is interacting with external objects, while the actuators are placed on the wrist of the human hand for the feedback mechanism (Figure 2.1C). The standalone electronic circuit serving as the core part of the e-skin system consists of a microcontroller unit (MCU) together with other electronic components to receive the data from the sensors, process the data, and send it to the actuators.

Figure 2.1D shows a fabricated single-pixel array of sensors having a total area of $1cm^2$ and contains four types of sensors. A microfabricated pyramid structure was placed on top of the pressure sensor which enhances the sensitivity of the sensor by maximizing the effective deformation of dielectric material. With the use of a pyramid structure, the applied force leads to a more pronounced change in the capacitance between the interdigitated electrodes, making the sensor more responsive to subtle pressure changes. Similarly, a ridge was attached to one side of the texture sensor, which applies tension on the sensor when subjected to the rough surface. To demonstrate the miniaturization

potential of the e-skin system using the microfabrication approach, a 2 x 2 array of sensors with the dimensions of (0.32 cm^2) was fabricated through simple spin coating and thermal evaporation processes (Figure 1E). The 2 x 2 array of sensors is as thin as 115 µm after the protection layer on top and bottom. Our fabrication design has the capability that the sensors array can be further miniaturized to have more sensors in a small area. We have shown that the same area (0.32 cm^2) can be utilized to fabricate a 3 x 3 array of sensors (Figure 2.2).

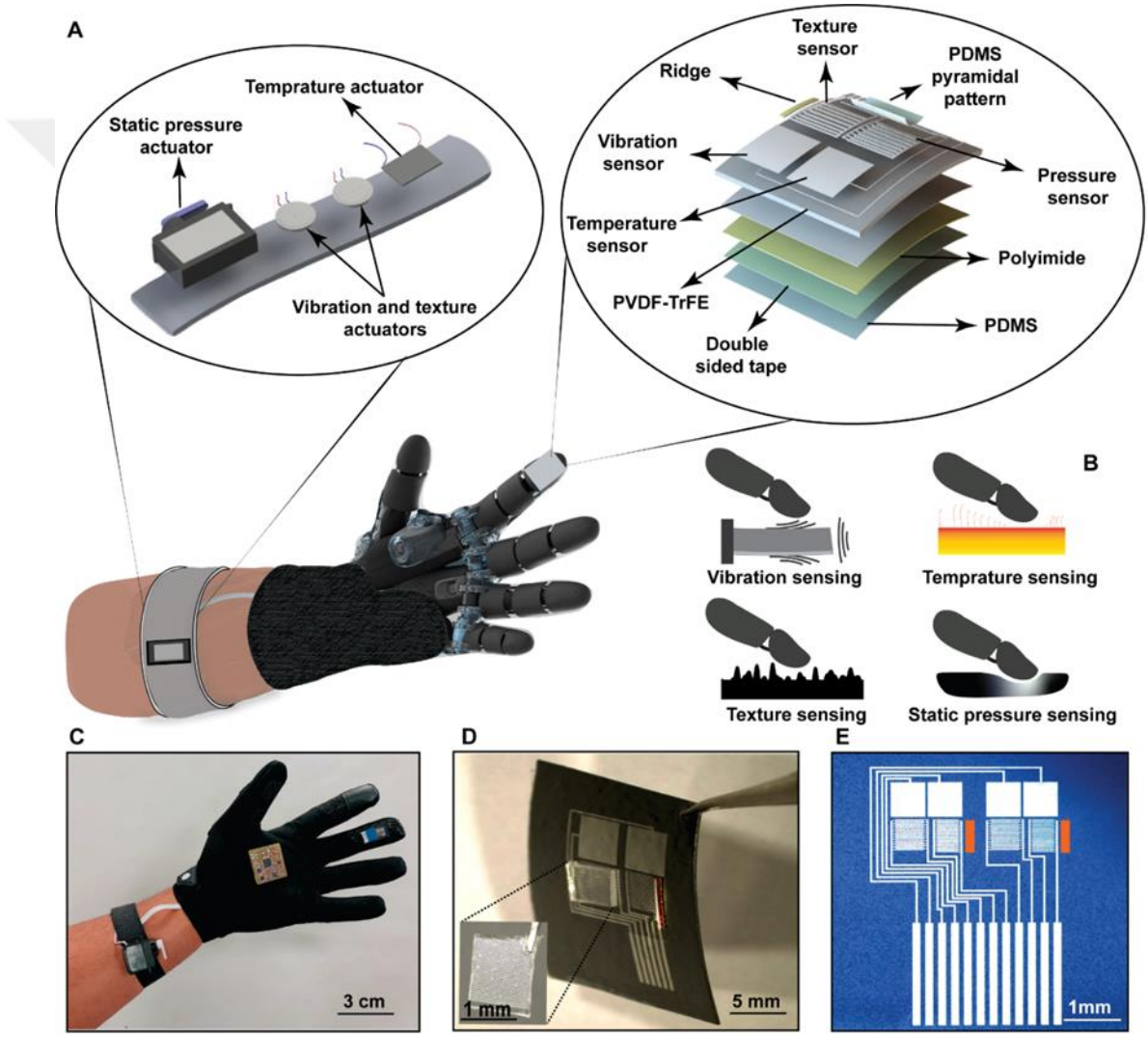

Figure 2.1 Schematic illustration and overview of a multifunctional sensory feedback Electronic Skin for the upper limb amputation. (A) Schematic illustration of our E-skin system. (B) Exploded view of the 2 pixels of miniaturized sensors containing different layers of the sensors. (C) Picture of the E-skin setup worn by a person with the glove to mimic the prosthetic hand and the Velcro on the wrist. (D) Picture of the E-skin system

attached to a glove. (E) Optical image of a single Pixel array of E-skin sensors highlighting its miniaturized and flexible form factor.

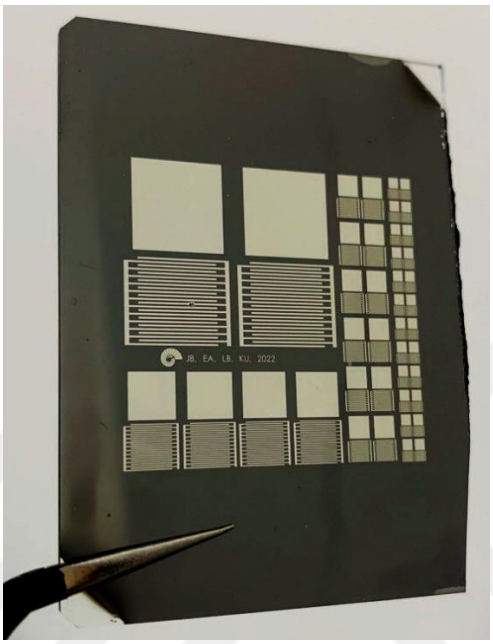

Figure 2.2 Photograph of the E-skin sensor arrays. The picture shows the process of miniaturization of the sensor array from a signal pixel to a two-pixel array of sensors.

2.2 Working mechanisms of the sensors

2.2.1 Pressure sensor

The applied external pressure leads to a change in output capacitance. According to formula (1), the capacitance can be changed by changing the area of the two plates, the distance between the two plates, and changing the ε_r of the dielectric layer.

$$C = (\varepsilon_0 \varepsilon_r A)/d \qquad (1)$$

Where, d, ε_0, ε_r, A represents the thickness of the dielectric, permittivity of the free space, permittivity of the dielectric, and area of the electrodes. The change in capacitance occurs due to the deformation of the dielectric layer. The pyramidal shape made of PDMS was placed on the sensor and the change in dielectric constant stemming from the geometrical shape change in the pyramidal structure. We selected PVDF-TrFE

(polyvinylidene fluoride -trifluoro ethylene) as a dielectric layer that possesses a relatively high dielectric constant compared to some other polymers. This property enhances the capacitance change between the sensor's interdigitated electrode arrays, making it more sensitive to pressure variations. When external pressure is applied, the interdigitated capacitive sensor exhibits a linear response, wherein the increase in capacitance corresponds directly to the magnitude of the applied pressure (Figure 2.3A). Figure 2.3B illustrates the scanning electron microscope (SEM) image of the interdigitated capacitive sensor. In contrast to a parallel plate capacitor, the interdigitated capacitor is capable of detecting variations in the material under test using only one side. This design offers a higher quality factor compared to the parallel plate capacitor.

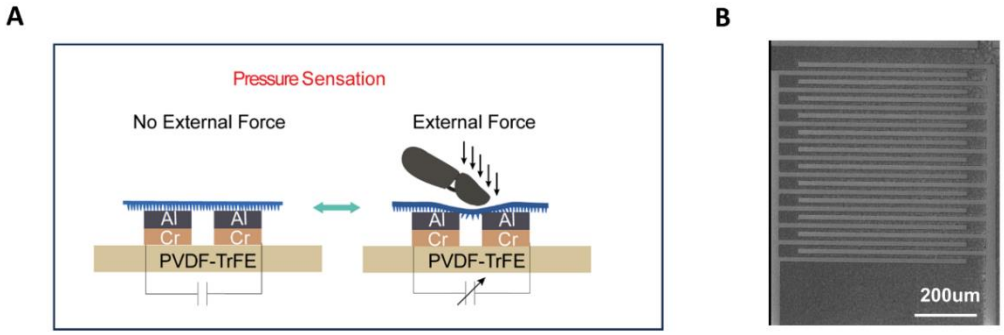

Figure 2.3 Performance characteristics of the pressure sensor and pressure actuator. (A) working principle of the pressure sensor. (B) Scanning Electron Microscopy (SEM) image of the miniaturized pressure sensor.

2.2.2 Temperature sensor

This sensor exhibits a change in capacitance in response to variations in the external temperature. By measuring this change in capacitance, we can effectively determine the temperature applied to the sensor. Figure 2.4A illustrates the working mechanism of the temperature sensor. The capacitance of this sensor is influenced by three key parameters:

the area of the electrodes, the distance between the electrodes, and the permittivity of the dielectric layer. These parameters collectively determine the capacitance of the capacitive sensor according to the formula (1)

As the external temperature changes, the relative permittivity of the dielectric layer in the sensor increases, resulting in a corresponding increase in capacitance. Figure 2.4B presents the SEM image of the top view of the parallel plate capacitive sensor.

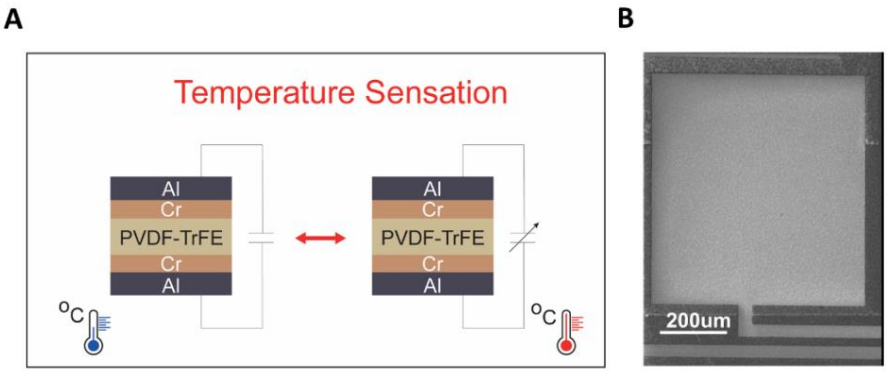

Figure 2.4 Performance characteristics of the Temperature sensor and actuator. (A) Working mechanism of the miniaturized temperature sensor. (B) SEM (Scanning electron microscopy) image of the soft temperature sensor.

2.2.3 Vibration sensor

This sensor detects external vibrations of varying frequencies and generates an output voltage in response. The sensor follows a parallel plate configuration, utilizing PVDF-TrFE (polyvinylidene fluoride -trifluoro ethylene) as the dielectric layer. Specific design details and the fabrication process are elaborated in the Materials and Methods section to provide further insights into the sensor's structure and construction. PVDF is a piezoelectric plastic material with a unique property: when subjected to mechanical deformation, it generates equal and opposite charges on both sides of the film. In the case of our piezoelectric-based vibration sensor, external vibrations cause the PVDF film to

align its dipoles in a specific direction, from the top layer to the bottom. This alignment results in the generation of voltages in the external circuit (Figure 2.5A). The amplitude of the voltage produced in the external circuit is directly proportional to the amplitude of the applied vibration. Hence, higher-amplitude vibrations induce higher-voltage outputs from the sensor. This behavior enables the sensor to accurately capture and quantify the magnitude of external vibrations based on the resulting voltage signals. Figure 2.5B presents a top-view scanning electron microscopy (SEM) image of the constructed piezoelectric-based vibration sensor.

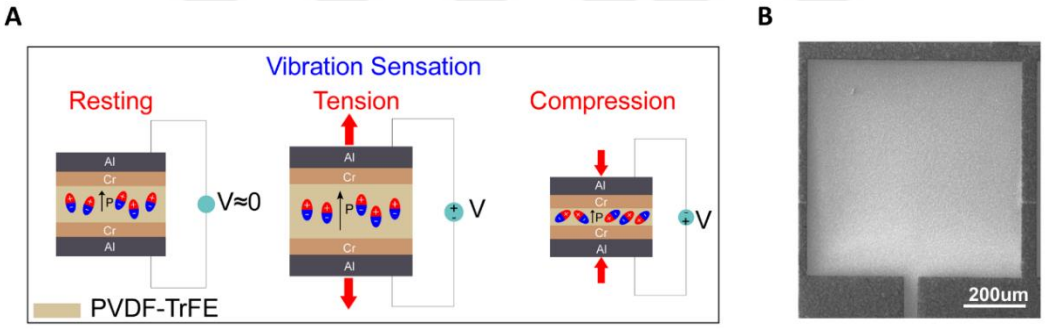

Figure 2.5 : Characterization of piezoelectric-based vibration sensor and actuator: (A) Working mechanism of the piezoelectric-based vibration sensor. (B) Scanning Electron Microscopy (SEM) image of the vibration sensor.

2.2.4 Texture sensor

In our design, we have incorporated an interdigitated piezoelectric sensor as the texture sensor. Our texture sensor is designed for detecting low-frequency rough textures. This sensor is capable of generating a voltage output when it comes into contact with an

external textured surface, allowing us to capture and analyze the tactile information of the surface. To enhance the detection of surface textures, a ridge made from Kapton tape was attached to the edge of the sensor surface. This ridge has specific dimensions, with a width of 0.3 mm and a height of 1 mm, providing a defined contact area for the sensor to interact with the textured surface. When the sensor slides on a rough surface, the ridge produces tension on the sensor, and the potential difference is generated between the IDE electrodes (Figure 2.6A). By analyzing the voltage output from the interdigitated piezoelectric sensor, our system can interpret the texture frequency information and provide haptic feedback to the users which enables them to perceive and distinguish different surface textures using a prosthetic hand. Figure 2.6B shows the top view of the SEM photo of the piezoelectric-based texture sensor with a ridge attached to its side.

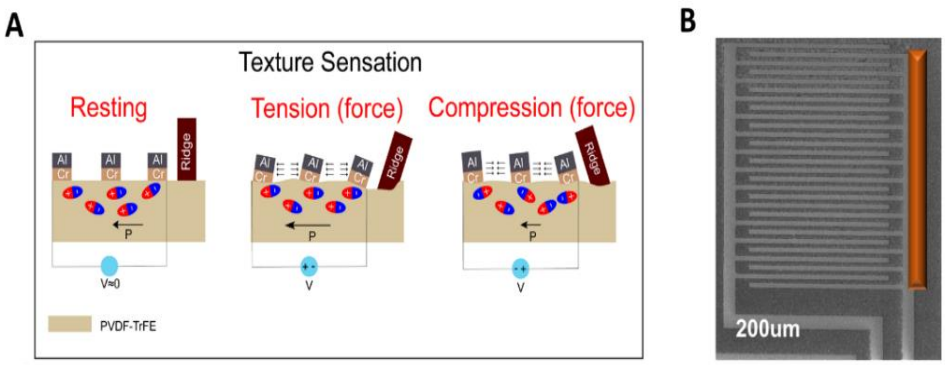

Figure 2.6 Performance characteristic of the piezoelectric-based texture sensor and actuator. (A) the working mechanism of the piezoelectric-based texture sensor. (B) SEM photo of the piezoelectric-based texture sensor.

2.3 Block diagram

Our e-skin system can be represented in three main subsystems: (i) a multiplexed piezoelectric sensor to gather haptic information during contact with an object; (ii) a miniaturized printed circuit board (PCB) that reads the data from the sensor and sends the data to the actuators; (iii) a velcro band that contains actuators to stimulate the healthy

area of the skin (Figure 2.7). The sensors and actuators used in this setup have a fast response time between the sensation by the sensors on the residual limb and the actuation on the human skin. The velcro attached to the upper limb provides a soft interface of the actuators to the skin which makes the system easy to use.

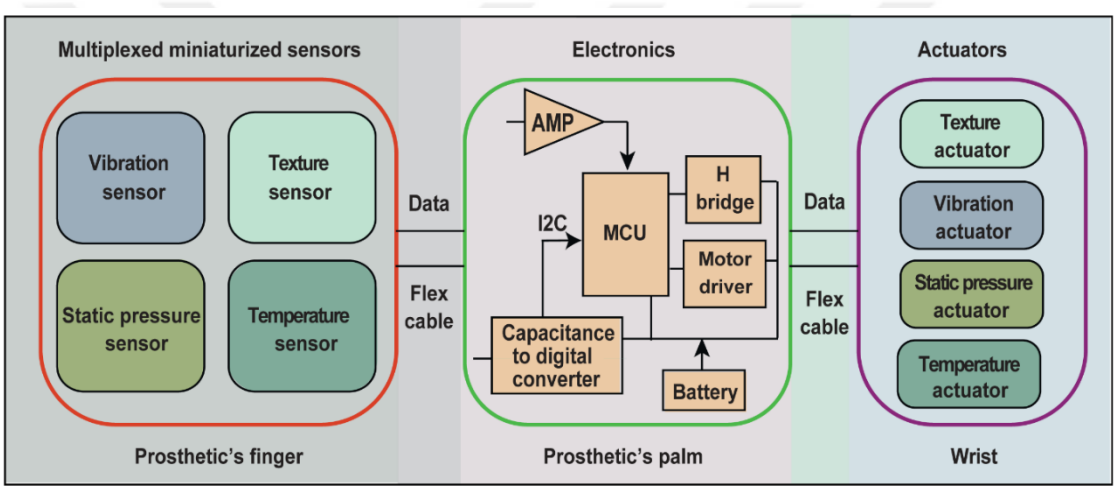

Figure 2.7 Functional Block diagram showing the E-skin system in three parts: Multiplexed, a piezoelectric-based array of sensors; a miniaturized electronic circuitry with flexible connection and actuators for each corresponding sensor.

2.4 Design of the miniaturized electronic circuit

We designed a miniaturized double-sided electronic circuitry for the e-skin system to make the system standalone (Figures 2.8 and 2.9). The circuit included two main sensing mechanisms of the output from the array of sensors. For the static pressure sensor and temperature sensor, the output is observed as a change in capacitance. This change in capacitance is read by the 4-channels capacitance to digital converter IC communicates

with the microcontroller via I2C protocol. The FDC1004 (Texas Instruments, USA) capacitance to digital converter (CDC) has a full-scale range of ±15 pF, with 0.5 aF resolution a programmable offset capacitance of up to 100 pF, and an active shielding signal output. The CDC has four multiplexed sensing channels and output rates up to 400 Hz. The vibration sensor and texture sensors produce output as a change in voltage which passes through internal ADC in the microcontroller to digitalize the signal at a sampling frequency of 400 Hz. The signal processing unit consists of an SMD (surface-mounted device) microcontroller (Atmega328p, Microchip Technology Inc.) with a crystal oscillator, resistors, and capacitors as peripheral components. The electronic circuitry communicates with the sensors and actuators through flexible cables. The PCB also contains electronic components for the actuators. The Peltier module is controlled by using an H-bridge (DRV8225, Texas Instruments Inc.) which controls the switches that deliver power to the load. To run the coin cell eccentric rotating mass (ERM) vibration motor, motor drivers (DRV2605, Texas Instruments Inc.) were used to communicate with the microcontroller through the I2C protocol. The PCB is connected to a rechargeable lithium-ion (Li-ion) battery (GlobTek Inc.) which powers the whole system.

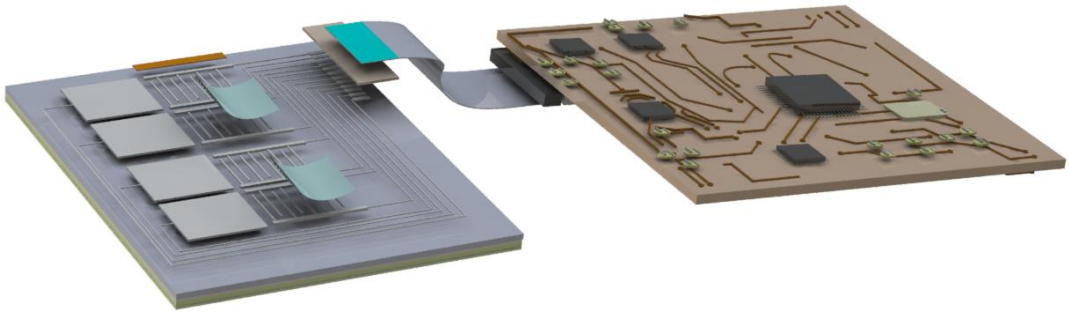

Figure 2.8 The schematic diagram of the e-skin sensors connected with the standalone printed circuit board (PCB).

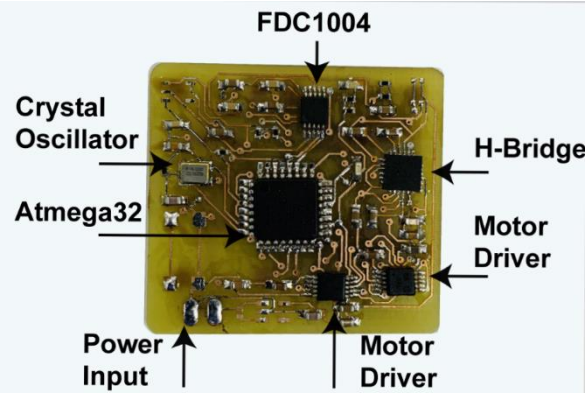

Figure 2.9 The actual picture of the fabricated miniaturized PCB with all the components mentioned.

2.5 Characterization of the actuators

2.5.1 Pressure actuator

According to the pressure-sensing characteristics of the biological skin, Human skin can sense a light touch in the pressure range from 0 to 10 kPa (Pan et al., 2014; Zang et al., 2015). To stimulate a gentle touch sensation on the human skin, a servo motor was utilized as an actuator. The servo motor was attached to a Velcro strip located on the wrist of the hand. The servo motor's arm undergoes controlled rotation to a designated angle in response to an external pressure leading to a variation in the sensor's initial capacitance. This rotation applies pressure within the range associated with a mild touch on the skin's surface where it's situated. This mechanism allows for the replication of a gentle tactile sensation similar to what the human skin can perceive. The actuator response can be seen in Figure 2.10. which shows the pressure produced by the servo motor while attached to a force transducer (Nano17, ATI Inc.). Indeed, the pressure exerted by the servo motor on the skin can be regulated by the external pressure applied to the sensor, resulting in a change in capacitance. As the rotating arm of the motor presses against the skin of the subject, a greater rotation away from the initial point toward the skin's surface corresponds to a higher applied pressure on the skin. By adjusting the external pressure

on the sensor, the desired level of pressure can be controlled and translated into the corresponding rotation of the servo motor, effectively modulating the pressure experienced by the skin.

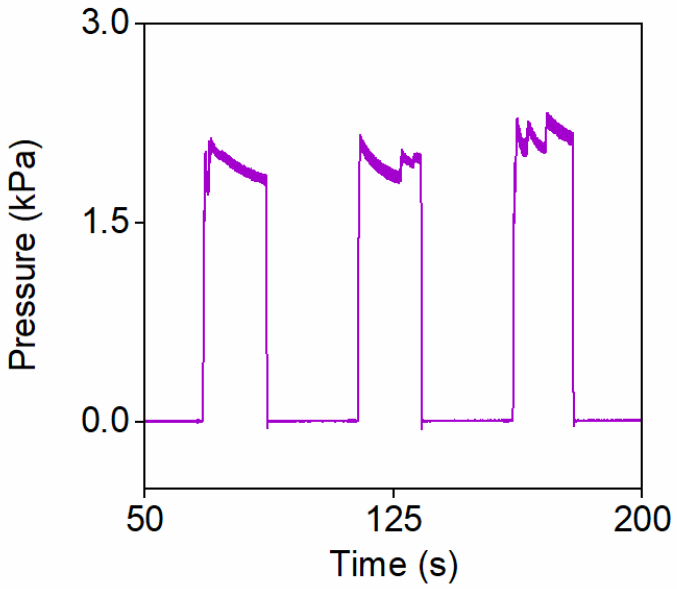

Figure 2.10 Response of the pressure actuator to produce a soft touch in response to the applied pressure of the sensor.

2.5.2 Temperature actuator

To generate a temperature sensation on the human skin, the temperature actuator was placed on the wrist of the human hand. In this setup, a Peltier module was utilized as an actuator, capable of generating a temperature difference between its two sides when a voltage is applied. When the capacitance of the sensor deviates from its initial value, a logic high signal is sent to a digital pin on the microcontroller. This signal triggers the actuator, thereby activating the Peltier effect and resulting in the desired change in temperature sensation on the skin. Given that the warm thermoreceptors of the human skin are typically stimulated in the temperature range of 25–40 °C (Q. Li et al., 2017), it is crucial for the actuators to respond swiftly within this range and for real-time communication to be established. Our setup defined four temperature ranges between 30

°C and 50 °C, each spanning 5 °C increments (Figure 2.11A). The actuator is stimulated only once within each range when the temperature is rising. The amplitude of stimulation increases as the temperature range becomes higher. However, during the falling temperature range, no stimulation is applied by the actuator. Figure 2.11B represents the characteristic curve of the actuator's temperature, whose temperature could be easily increased up to a high temperature with low voltage. The relationship between the voltage and the final maintained temperature is plotted. As the PWM (pulse width modulation) signal stimulation is given to the actuator, the voltage output to the actuator is controlled by the H-bridge.

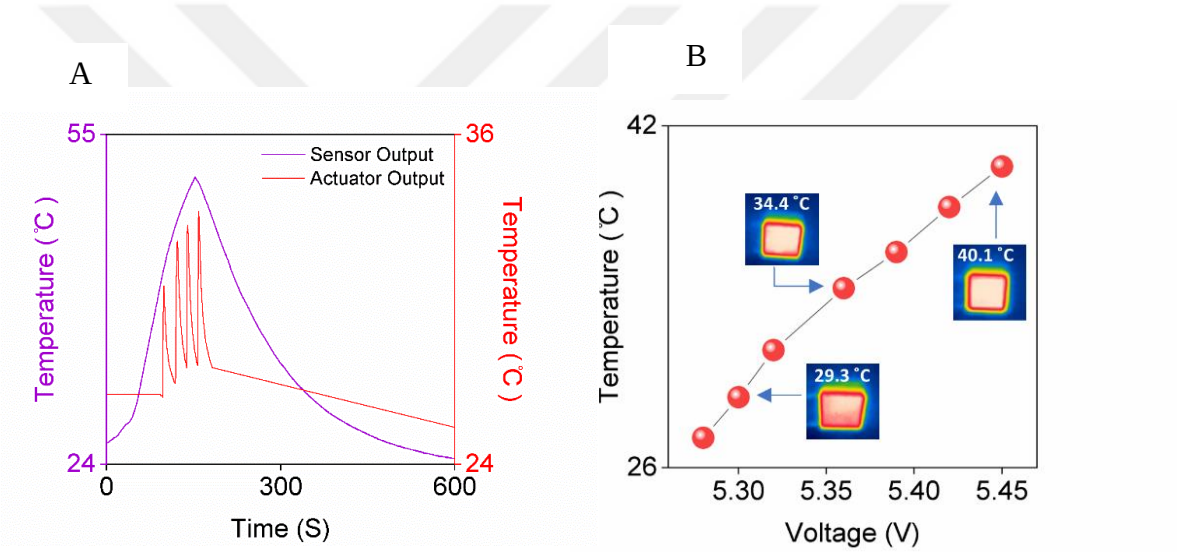

Figure 2.11: Temperature actuator response. (A) The figure illustration of the relation between the temperature sensor and temperature actuator. (B) The output of the temperature actuator to the increase in applied voltage.

2.5.4 Vibration actuator

In our e-skin system, actuation plays a vital role and complements the sensor output. To create the sensation of vibration on the skin, we incorporated coin cell vibration motors as vibration actuators (Jung et al., 2022b). These eccentric rotating mass (ERM) motors (VC1026B002F, Vybronics, Inc.) were specifically chosen to vibrate at the same

dominant frequencies produced by the vibration sensor. To synchronize the actuation with the sensor output, we utilized a motor driver (DRV2605, Texas Instruments Inc.). The motor driver generated a PWM signal that was mapped with the dominant frequency obtained from the real-time FFT analysis conducted in the microcontroller. This mapped PWM signal was then used to drive the vibration motors, ensuring that they vibrated at the desired frequency. For vibration actuation, both motors operated simultaneously with the same PWM signal. Figure 2.12A and Figure 2.12B demonstrate the operation of the two motors vibrating at 100 Hz and 80 Hz, respectively, with synchronized PWM. This synchronized vibration actuation provides a realistic and coordinated vibration sensation to the user's skin.

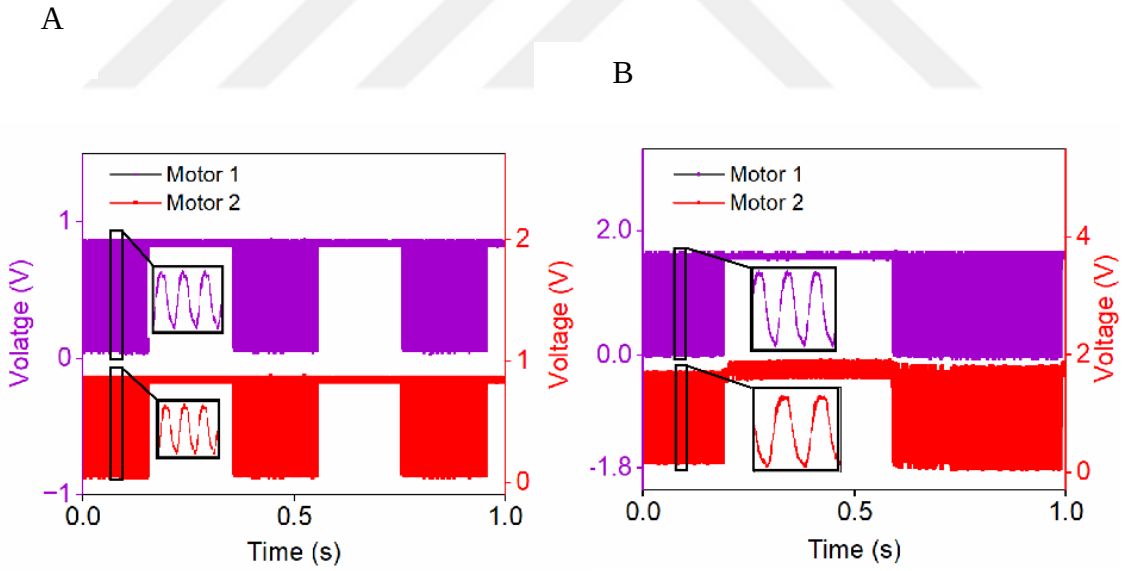

Figure 2.12: Output response of the vibration actuator. (A)PWM output of two coin-cell motors vibrating simultaneously with the frequency of 100 Hz. (B) PWM output of two coin-cell motors vibrating simultaneously with the frequency of 80 Hz.

2.5.5 Texture actuator

To produce the sensation of texture on the healthy part of the human body, we used two coin-cell vibration motors. The motors were given a PWM signal with a certain delay between the actuation time, as shown in Figure 2.13. The delay between the actuation time of the two motors corresponds to the roughness of the texture on which the sensor is sliding. In this figure, 'I' represents the off time of the motor, and 'h' represents the time delay between the actuation of two motors which corresponds to the spatial period of the surface.

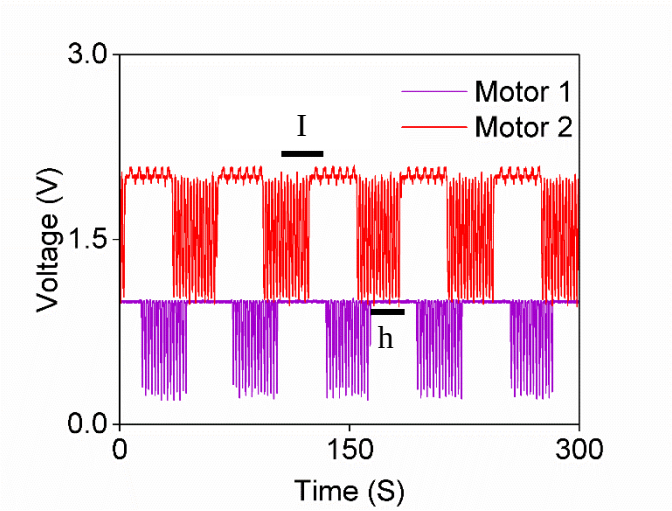

Figure 2.13: PWM signal of two vibration motors vibrating with a certain delay.

Chapter 3: **IN VITRO EXPERIMENTS**

3.1 Characteristics of pressure sensor

The manufacturing process involved the creation of a miniaturized sensor array, specifically designed with two-pixel sets, each containing four individual sensors. These sensors encompassed a diverse range of functionalities, including the measurement of static pressure, temperature, vibration, and texture.

Of particular significance is the static pressure sensor within this array. It was meticulously crafted to incorporate a multi-finger periodic structure, which encompasses interdigitated capacitive sensors. These sensors are conceptually represented by lumped circuit elements, a modeling approach that simplifies the complex physics involved in the capacitive sensing mechanism.

Remarkably, the static pressure sensors showcased a variety of critical attributes. They demonstrated a rapid response rate, allowing them to swiftly detect and transmit pressure variations. Additionally, their hysteresis, which refers to the lag in response when pressure changes, was minimized, leading to highly accurate measurements. The sensors also exhibited outstanding linearity, ensuring that their output was directly proportional to the applied pressure. Long-term stability was another notable feature, indicating that the sensors maintained their accuracy and performance over extended periods of use. Lastly, these sensors boasted a wide operational range, implying that they could effectively function across a broad spectrum of pressure levels.

Collectively, this sensor array represents a sophisticated technological achievement, encompassing diverse sensing capabilities and leveraging advanced engineering principles. The static pressure sensors, with their intricately designed multi-finger structure and advantageous characteristics, epitomize the cutting-edge nature of this sensor array's development.

3.1.1 Linear response of the pressure sensor

The designed pressure sensor results in a change in capacitance with the applied external pressure. The measured capacitance is a linear function of pressure and remains unchanged when the applied pressure remains constant (10 KPa) (Figure 3.1).

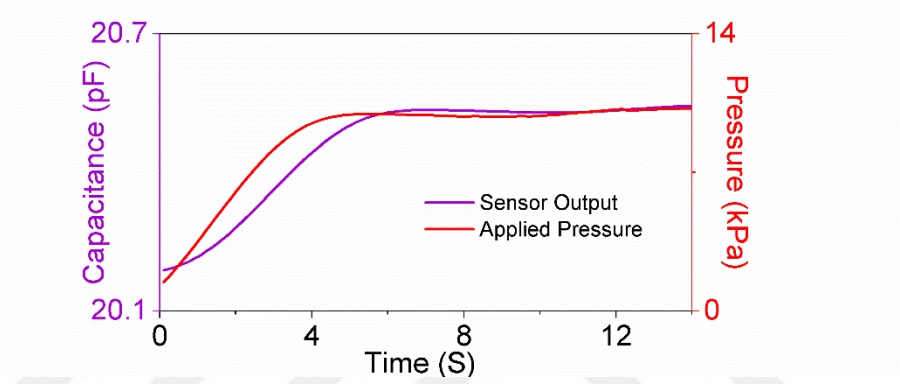

Figure 3.1: Linear response of the sensor. Change in capacitance (Delta C) with respect to the applied.

3.1.2 Loading/Unloading test.

To record the change in capacitance resulting from the applied pressure on the sensor, an impedance analyzer (MFIA, Zurich Instruments, Zurich Switzerland) synchronized with a force gauge was employed. The force gauge was used to apply pressure on the sensor while the impedance analyzer measured and recorded the corresponding change in capacitance. Under cyclic loading and unloading, the capacitance of the interdigitated capacitive sensor varies as expected in response to the applied pressure. When the force was applied, the capacitance changed accordingly, and upon removal of the force (when it becomes zero), the capacitance returned to its initial value (Figure 3.2A). Figure 3.2 B shows the extracted calibration curve is linear for different applied external pressures, ranging from 1 kPa to 10 kPa. Subsequently, the sensor was connected to the miniaturized electronic circuitry using a flexible cable. A loading/unloading test was conducted, during which the change in capacitance was recorded utilizing the capacitance to digital converter IC (FDC1004). Figure 3.3 illustrates the anticipated response of the pressure sensor to cyclic loading and unloading, demonstrating that the sensor's capacitance promptly returns to its initial value without any noticeable delay.

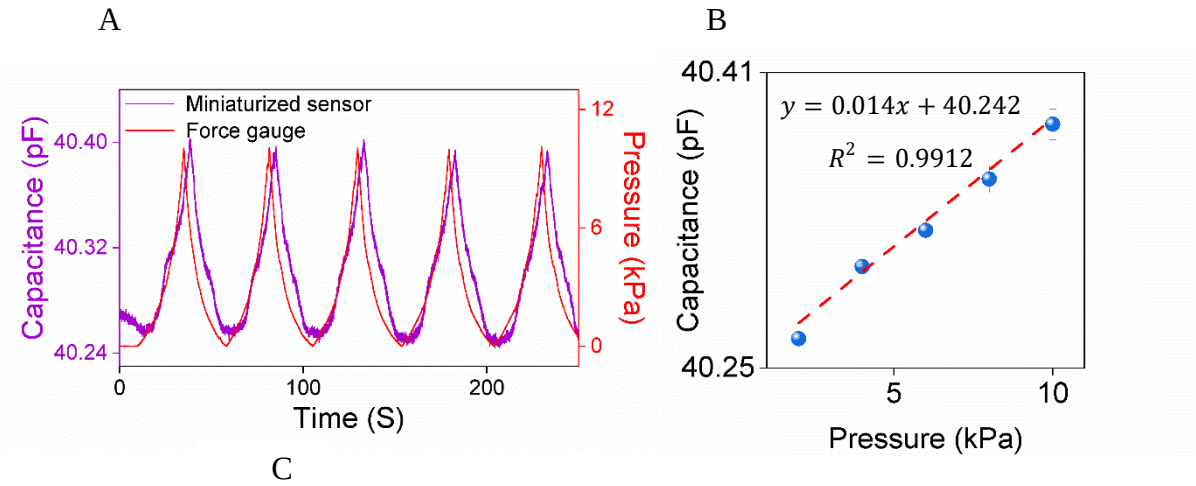

Figure 3.2: (A) Change in capacitance of the sensor under four cycles of loading/unloading compared to the measurements using a force gauge. (B) Extracted calibration curve of the device.

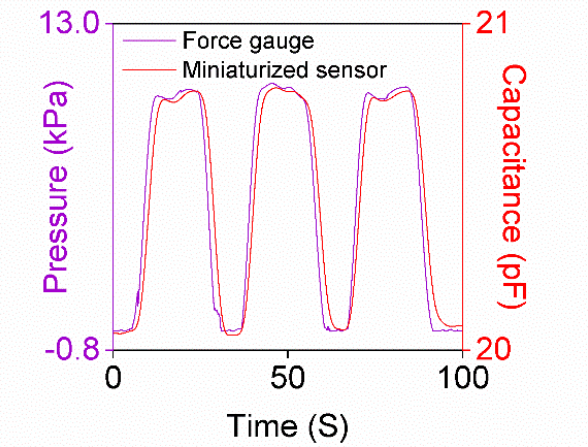

Figure 3.3 Change in capacitance of the sensor connected to the electronics under three loading/unloading cycles compared to the measurements using a force gauge.

3.2 Characteristics of temperature sensor

The temperature of the human body can be monitored using wearable and flexible sensors. In our case, we developed a temperature sensor utilizing a parallel plate capacitive configuration.

3.2.1 Linear response

The sensor was connected to the impedance analyzer to record the change in capacitance due to the applied temperature. The change in applied temperature leads to the change in the capacitance of the sensor, which can be demonstrated in the form of the linear relationship between the change in capacitance and the applied external temperature (Figure 3.4).

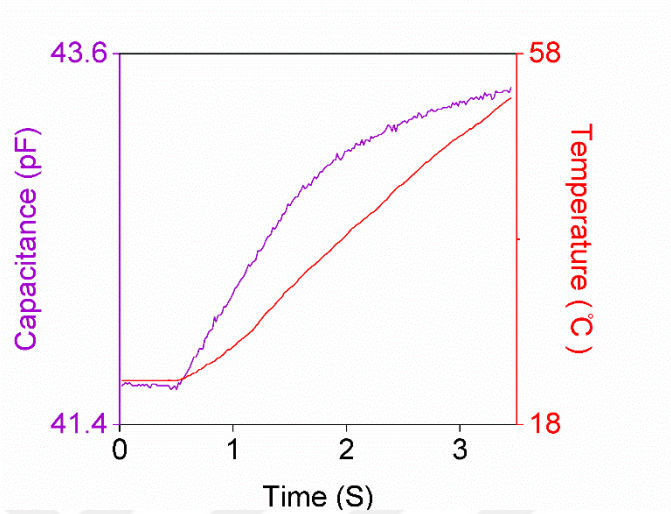

Figure 3.4 Linear response of the temperature sensor with the applied temperature.

3.2.2 Comparison with a commercial sensor

The output of the sensor was monitored as a change in capacitance as a result of applied external temperature. Figure 3.5 demonstrates the capacitance response of the fabricated temperature sensor to the externally applied temperature. The sensor exhibits a promising response to the external temperature which ensures the sensor's functionality. The output of the sensor was compared with the commercial temperature sensor (MPL3115A2, NXP USA Inc.) by applying external temperature to both the fabricated sensor and commercial sensor simultaneously.

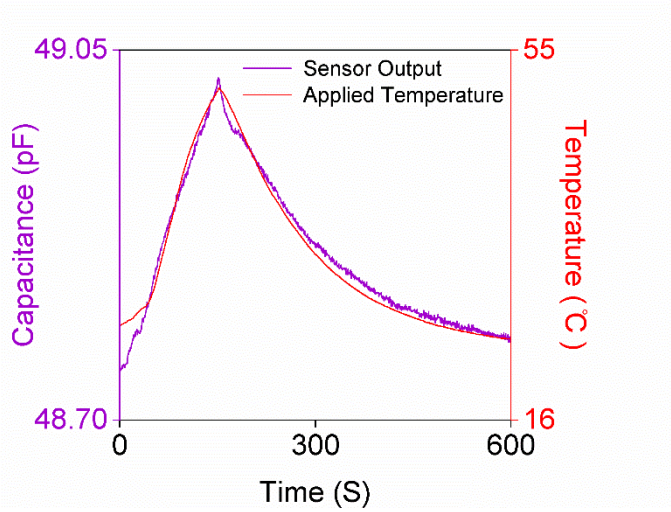

Figure 3.5: variation of capacitance with the applied external temperature to the sensor.

3.2.3 Sensor connected to the electronics.

The sensor was then connected to the standalone miniaturized electronics to record the change in capacitance by using a capacitance-to-digital converter IC (FDC1004, Texas Instruments, USA). The fractional change of the analog-to-digital converter (ADC) values acquired from the miniaturized PCB is presented in response to different temperatures (Figure 3.6). The change in temperature, ranging from approximately 30 °C to 50 °C, was correlated with the corresponding change in capacitance when the temperature was applied to the miniaturized sensor. This comparison is made with a commercial sensor. The data obtained from the miniaturized sensor shows good agreement with the readings from the commercial sensor.

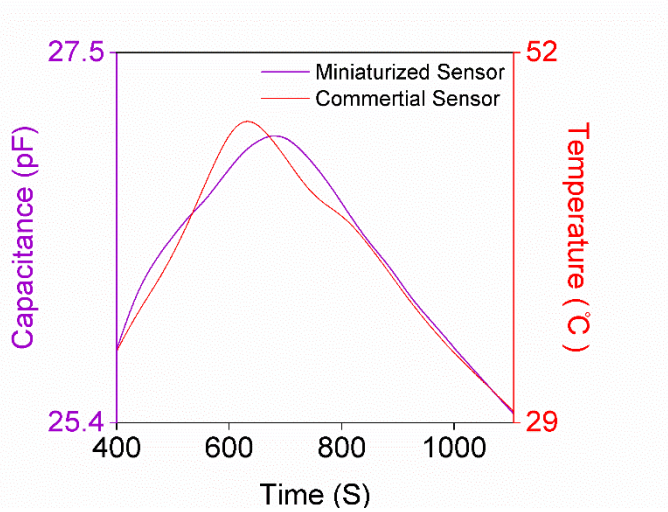

Figure 3.6: Response of the miniaturized temperature sensor to the external temperature in comparison with the commercial sensor.

3.3 Characteristics of vibration sensor

Our skin exhibits heightened sensitivity to mechanical vibrations within the frequency range of 40 to 400 Hz (Chun et al., 2016; Vicentini et al., 2010). To replicate the vibration-sensing ability of human skin, we designed a piezoelectric-based vibration sensor.

3.3.1 Output of vibration sensor as voltage waveform

To induce vibrations, the sensor was subjected to a vibrating beam with a vibration motor attached underneath it (Figure 3.7). The output of the piezoelectric vibration sensor was connected to an oscilloscope to record the data in the form of an output voltage signal. The voltage signal recorded with an oscilloscope with a sampling frequency of 100 kSa/S, is presented in Figure 3.8A for 10 seconds. To eliminate any 50 Hz environmental noise, the signal was passed through a notch filter with a notch frequency of 50 Hz. To validate the vibration sensor's capability to detect a wide range of frequencies, high-frequency

vibrations were applied to the sensor. Figure 3.8B depicts the resulting voltage signals generated by increasing the external vibration to 80 Hz and the voltage waveform was obtained. Similarly, applying another external vibration 100 Hz to the sensor and the voltage waveform was obtained (Figure 3.8C). This experiment shows the functionality of our sensor to the wide range of external vibrations.

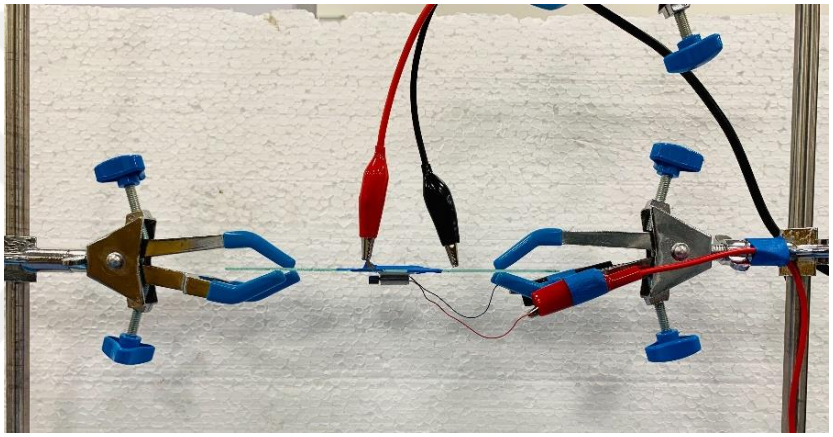

Figure 3.7 Experimental setup of the vibration sensor.

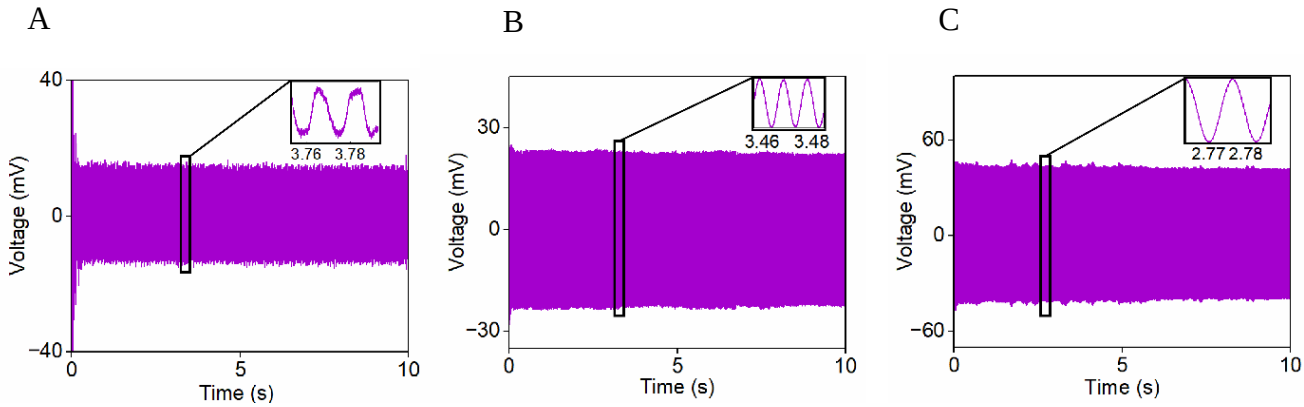

Figure 3.8 Voltage output of the vibration sensor. (A) The voltage waveform of the output signal of 60 Hz vibration. (B) The output of the sensor when subjected to the external vibration of 80 Hz. (C) The 100 Hz vibration output of the vibration sensor.

3.3.2 FFT response of the output signals

To confirm the vibration sensor's frequency, a fast fourier transform (FFT) analysis was performed using MATLAB. The resulting FFT plot in Figure 3.9A reveals the dominant frequency in the output signal to be 60 Hz, validating the vibration sensor's generated frequency. To confirm the dominant frequency present in these signals, we conducted FFT analysis in the MATLAB. Figure 3.9B displays the FFT signal of waveform 3.8B, showing a dominant frequency of 80 Hz. Similarly, for the waveform obtained in Figure 3.8C, FFT analysis revealed a dominant frequency peak at 100 Hz, as illustrated in Figure 3.9C. These analyses demonstrate the vibration sensor's accurate capturing and differentiation of various frequencies within its operating range, including lower and higher frequencies.

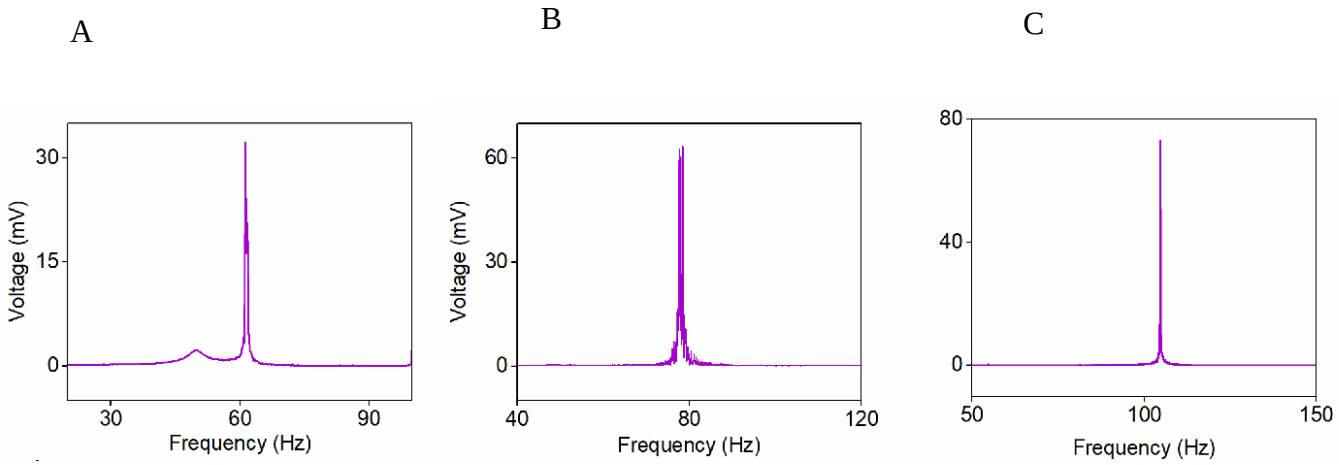

Figure 3.9: Fast Fourier Transform (FFT) response of the output signals. (A) dominant frequency of 60 Hz obtained from the voltage waveform. (B)The dominant peak of 80 Hz calculated from the 80 Hz vibration waveform. (C) The FFT response of the 100 Hz voltage waveform.

3.3.3 Comparison of the sensor with a commercial sensor

We conducted a performance comparison with a commercial accelerometer to verify the dominant frequency produced by our vibration sensor. Both the vibration sensor and the accelerometer were placed adjacent to each other on the vibrating beam and connected to an oscilloscope. The output of the accelerometer was recorded in the form of voltage waveform recorded at a sampling frequency of 100 kSa/s (Figure 3.10A). To confirm the dominant frequency, FFT analysis was performed on both waveforms. The FFT analysis revealed a dominant frequency of 80 Hz for both the vibration sensor and the accelerometer, indicating consistency between the two measurements (Figure 3.10B). Furthermore, to confirm the sensor's dominant frequency of 100 Hz, the output of the accelerometer was also obtained (Figure 3.10C). The FFT analysis was performed on the voltage waveform, and the 100 Hz frequency was confirmed (Figure 3.10D). The comparison of the fabricated sensor with the commercial sensor confirms the functionality of the sensor.

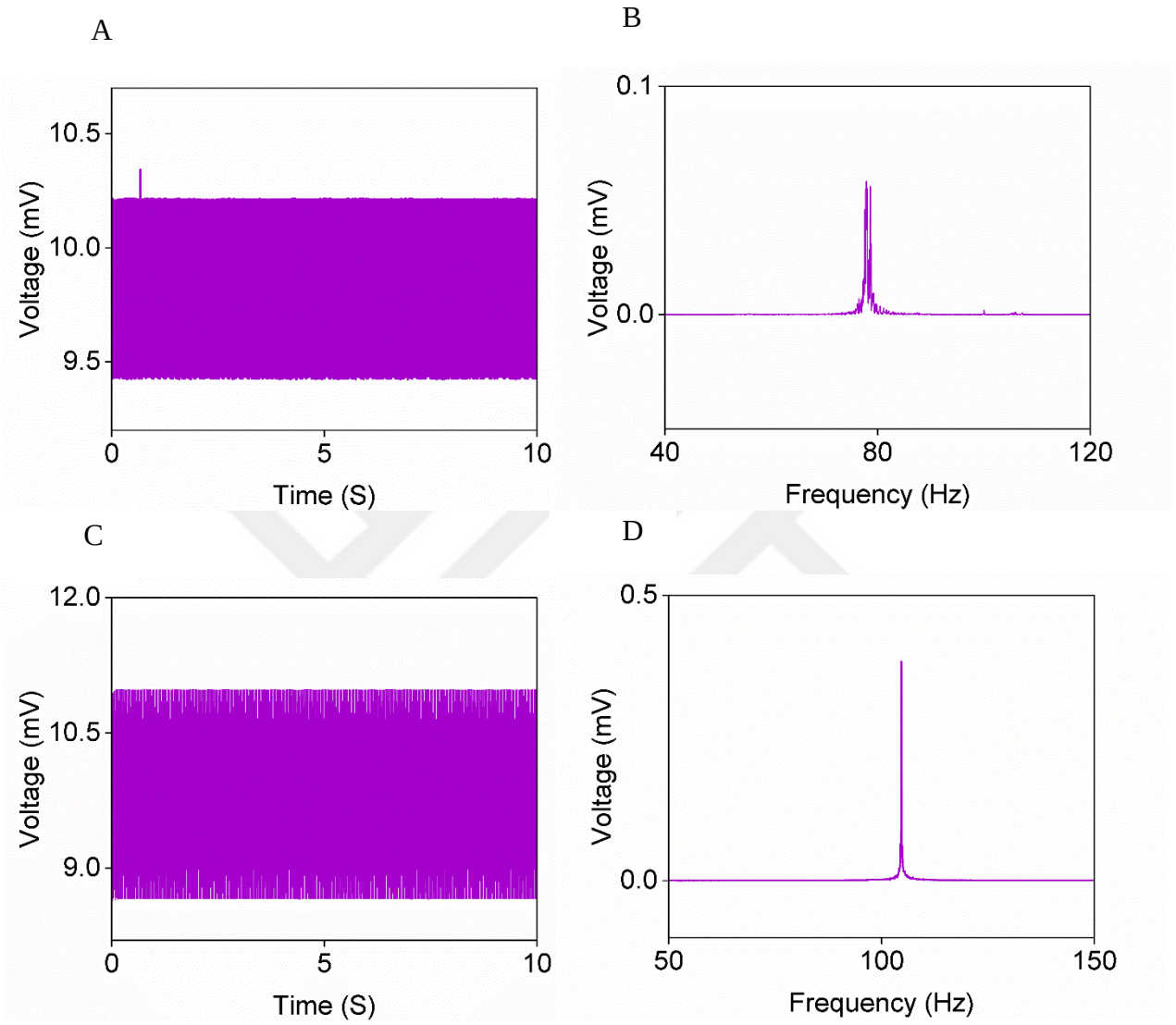

Figure 3.10: accelerometer output when subjected to the external vibration for comparison with the sensor. (A) The voltage waveform of the accelerometer when subjected to 80 Hz external vibration. (B) The FFT response of the 80 Hz waveform to confirm the dominant frequency. (C) The voltage waveform of the accelerometer when subjected to 100 Hz external vibration. (D) The FFT response of the 100 Hz waveform to confirm the dominant frequency.

3.3.4 *Sensor connected with the electronic.*

To evaluate the performance of the stand-alone system, we connected the vibration sensor to the miniaturized double-sided printed circuit board (PCB) specifically designed for our e-skin system. In this setup, we conducted a real-time FFT analysis of the input signal received by the microcontroller from the sensor. Figure 3.11 illustrates the output signal produced by the microcontroller, which involves identifying the dominant frequency using FFT analysis. This dominant frequency was further validated by comparing it with the output FFT signal obtained from the accelerometer. By comparing the FFT signals from both the microcontroller output and the accelerometer, we can confirm the accuracy and consistency of the dominant frequency determined by our standalone system. This analysis ensures that the system effectively captures and processes the vibration data, providing reliable information about the dominant frequency.

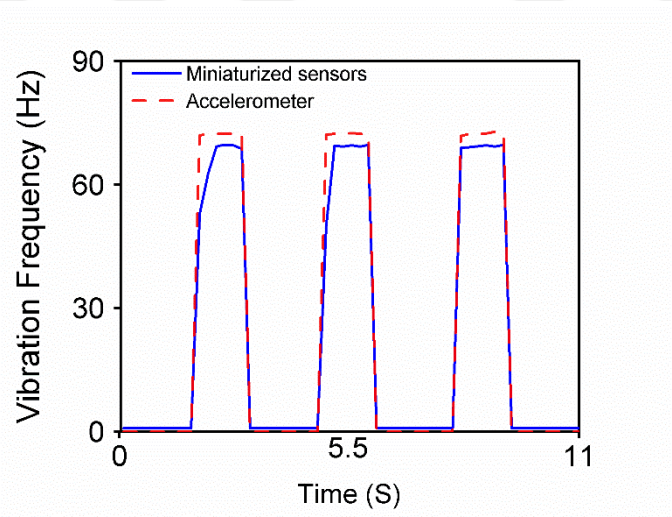

Figure 3.11: FFT output of the sensor and the accelerometer connected to the standalone electronics.

3.4 Texture sensor

There are two types of textures that human skin can sense; coarse textures, which are perceived by slow adapting mechanoreceptors and have a feature size of >100 um, and fine textures, which are perceived by rapidly adapting (RA) mechanoreceptors and have a feature size of <100 um. Fine textures are detected by fast adaptive receptors which are sensitive to the vibration generated by the relative motion between the skin and the object when sliding the finger over its surface (Sotgiu et al., 2020). Because of different depths and patterns, each texture produces unique data when moving on the surface of a sensor.

3.4.1 Sensor output as a voltage waveform

In the texture sensor experiment, the rough surface was placed at a moving stage (LTS150, Thorlabs Inc.) containing a force sensor (Mini40-SI-80-4, ATI Inc.) with a controlled speed, and the sensor was placed on a fixed point to be in contact with the surface (Figure 3.12). The voltage waveform was obtained by reading the output through an oscilloscope with a sampling frequency of 100 kS/s. The frequency obtained from the roughness of the surface depends on the spatial period of the texture and the speed with which the sensor is moving on a surface. The frequency can be determined from the following equation (2):

$$f = \frac{v}{\lambda} \qquad (2)$$

Where f is the characteristic frequency, v is the sliding speed, and λ is the period width (feature size) of the texture. With a fixed rate of 10 mm/s, a frequency of 2.5 Hz was obtained by making the spatial period 4 mm (Figure 3.13A). Similarly, the voltage waveform was obtained by increasing the moving speed to 20 mm/s while keeping the roughness of the surface with a spatial period of 4 mm (Figure 3.13B).

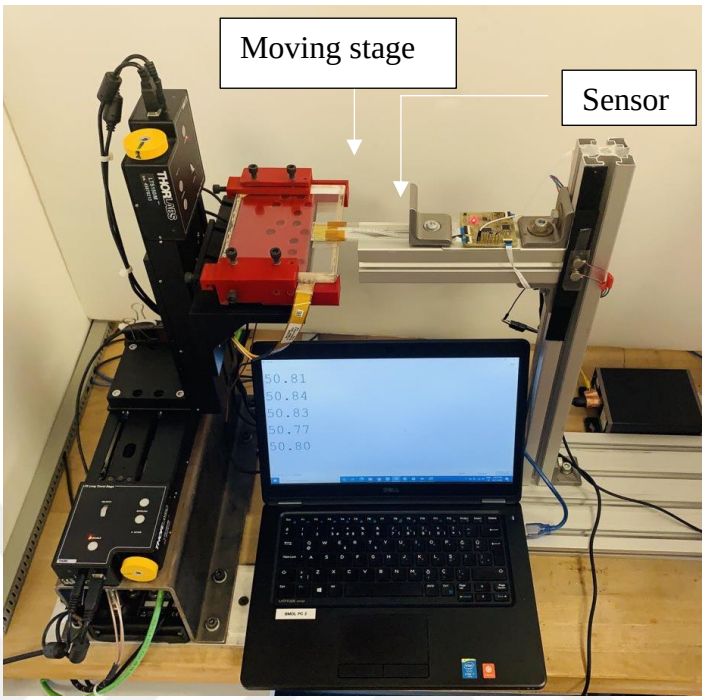

Figure 3.12 The experimental setup of the texture sensor.

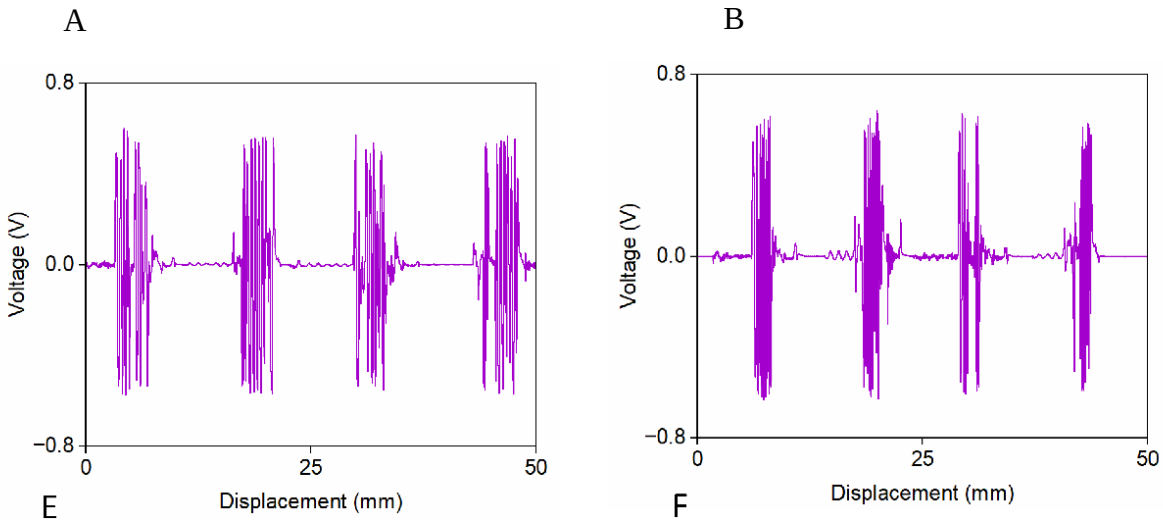

Figure 3.13: Output of the piezoelectric texture sensor. (A) Voltage waveform of the 2.5 Hz texture. (B) Output voltage waveform of the 5 Hz texture

3.4.2 FFT response of the output waveform

The dominant frequency was calculated by taking the FFT in MATLAB with the notch filter of 50 Hz to remove the noise from the signal (Figure 3.14A). The dominant frequency was calculated by taking the FFT of the signal which confirms the frequency of 5 Hz (Figure 3.14B). The fabricated sensor is capable of generating higher frequencies which depend upon the moving speed and the roughness of the surface. We moved the sensor on a rough surface two times with different moving speeds, and two different frequencies, 16 Hz and 18 Hz were obtained. These experiments demonstrate the accurate detection of both the low and high frequencies textures which shows the excellent performance of our sensor.

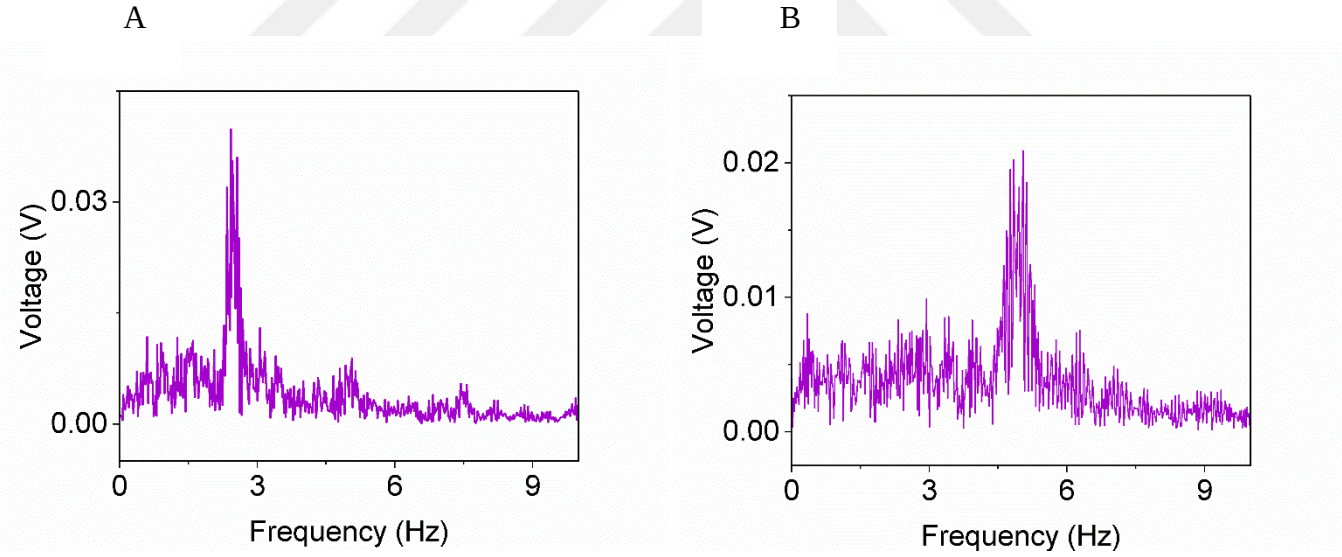

Figure 3.14: The FFT response of the texture signals. (A) The dominant frequency of 2.5 Hz was confirmed from the FFT response. (B) The dominant frequency of 5 Hz was confirmed from the FFT output.

3.4.3 Sensor connected with the electronics.

The miniaturized array of sensors was then connected to the electronics by using a flexible cable connection to get the data from the sensor. The real-time FFT was performed at 400 Sa/s in the microcontroller to detect the dominant frequency of the sensor. Figure 3.15 illustrates the two frequencies of 20 Hz and 30 Hz obtained by moving the sensor on texture surfaces (the surfaces are shown in the top left corner of the figure) having the roughness of 1 mm and 0.66 mm, respectively, with a constant speed of 20 mm/s.

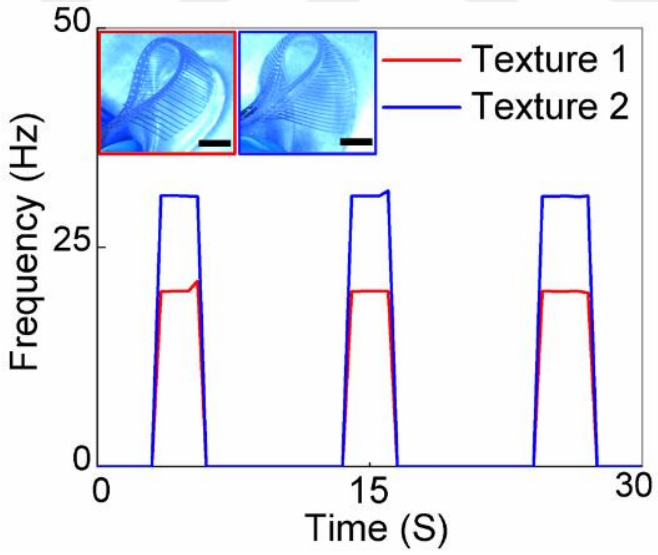

Figure 3.15: FFT output of two different frequencies produced by two different textures by using a microcontroller in the standalone electronics circuit.

Chapter 4: **IN VIVO EXPERIMENTS**

Validation trials of the E-skin system on human subjects demonstrate the performance and operational robustness of the system under controlled conditions. Tests involve mounting the e-skin system to the upper limb of healthy volunteers (n=10; Figure 4.1A) with a different age group. The multiplexed array of the sensors was placed on the middle finger, but the sensors array can be placed on any of the fingers of the hand. These locations are important parts of the hand for object manipulation and get sensation when in contact with an object. The participants were wearing a thick glove to isolate the system and prevent the sensations directly on the human skin, and the sensors array was placed on the finger of the glove. The sensor array was connected to the miniaturized electronics by using a flexible cable coming under the glove to reduce the bulkiness of the system. Upper limb amputation is considered to be an amputation in which a person loses their hand below the wrist. To translate the artificial sensation from the prosthetic hands to the healthy part of the upper hands, the wrist is to be considered the most sensitive to perceive the sensations. The array of actuators was placed on the wrist of the human by using a hook fastener (Velcro) to hold the actuators and connected to the miniaturized electronics (3 x 3 cm) through a flexible cable. Next, the participants were guided to wear a facemask and headphones with noise-canceling capabilities while playing white noise to prevent any external sounds from the device or surroundings that could potentially impact the perception of haptics. Since we report four distinct types of sensors, the experiment necessitates four corresponding tests for each sensation. Each experiment was repeated ten times with random patterns of the applied sensations for every participant. An embodiment questionnaire was prepared and presented to the participants to capture their responses qualitatively. At the end of each experiment, participants were asked to complete the questionnaire. Figure 4.1B depicts the setup for the temperature sensor experiment. The external temperature is administered to the sensor through a heat gun, while the actuator is positioned on the wrist of the hand. For the texture sensor experiment (Figure 4.1C), the surface was placed on a moving stage (Thor lab) and set to slide at a constant velocity. Participants were instructed to place their hands on a fixed point on the sliding surface. Regarding the feasibility trials for the vibration sensor, the sensor was situated on a beam subject to controlled vibration. Concurrently, the actuator was placed

on the wrist of the hand, as shown in Figure 4.1D. Furthermore, Figure 4.1E demonstrates the setup for the pressure sensor experiment. The pressure was exerted on the sensor using a force gauge while the actuator remained positioned on the wrist.

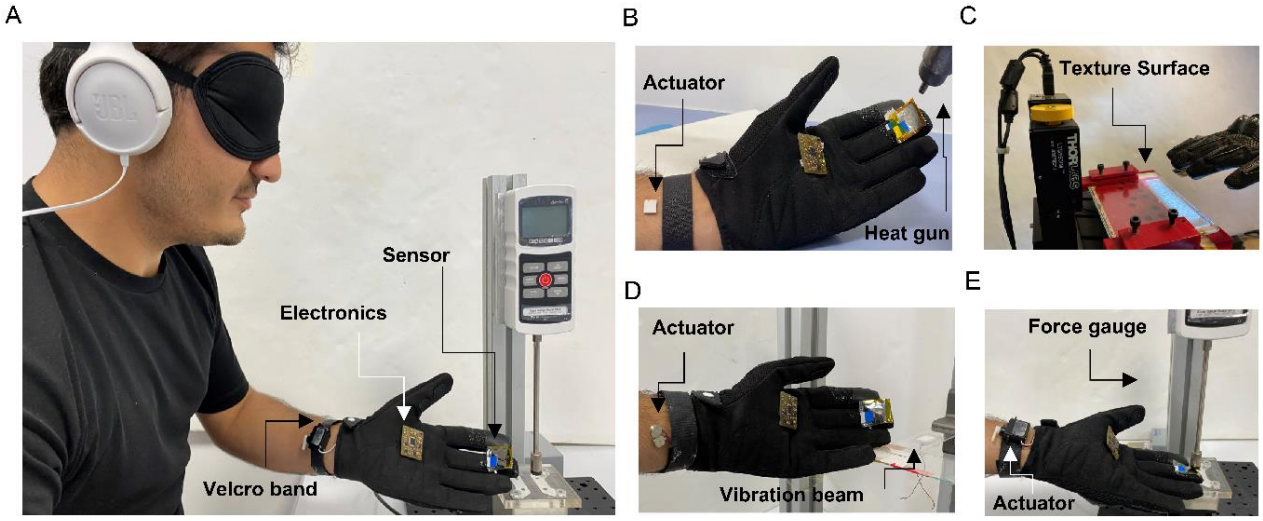

Figure 4.1: In vivo trial of the E-skin system on a human subject. (A) Photograph of the subject performing the experiments, the participant was blindfolded and acoustically shielded. (B) Experimental protocol for the temperature sensor while applying temperature by heat-gun. (C) Experimental protocol for the texture sensor by sliding the sensor on a textured surface. (D) Experimental protocol of the vibration sensor by sensing the vibration of known frequency. (E) The experimental protocol of the pressure sensor subjected the sensor to the force gauge.

4.1 Static pressure experiment

Pressure sensation and feedback mechanism are important functions to provide users with a more comprehensive perception of the object. Here, we performed an experiment on the pressure sensor by applying pressure to the sensor, and the actuator is attached to the human wrist. The applied pressure to the sensor with the pattern of the first three soft touches (~10 KPa) on the sensor followed by two touches and then one touch for a long period. The output of the sensor can be recorded in the form of a change in capacitance when the pressure is applied which different pattern as shown in Figure 4.2A. The three patterns of pressure were applied to each subject ten times randomly. The change in applied pressure resulted in the change in capacitance which was mapped to the rotation of the arm of the servo motor (pressure actuator) to produce a soft touch sensation on the human skin. The participants were asked to differentiate the applied pattern in the form of a questionnaire based on which statistical analysis was carried out. Overall, the ten participants correctly identified the three different patterns of applied pressure in 96.7 % of cases (Figure 4.2B). Based on the confusion matrix, sensitivity, and specificity values were calculated (Figure 4.3 A and B). The experiment demonstrates that the e-skin system performs well, as evidenced by its high sensitivity score (SE = 0.97) and specificity score (SP = 0.98). This confirms the effectiveness of the e-skin system.

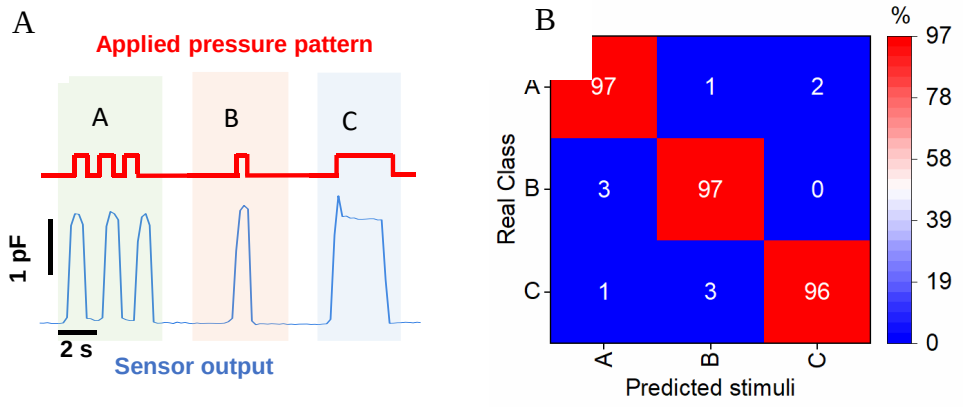

Figure 4.2: (A) Picture of the applied pressure sensor and the output response of the sensor. (B) The performance was obtained during a control condition where a pressure experiment was performed in the form of a confusion matrix. In every case, 30 repetitions were performed with ten participants.

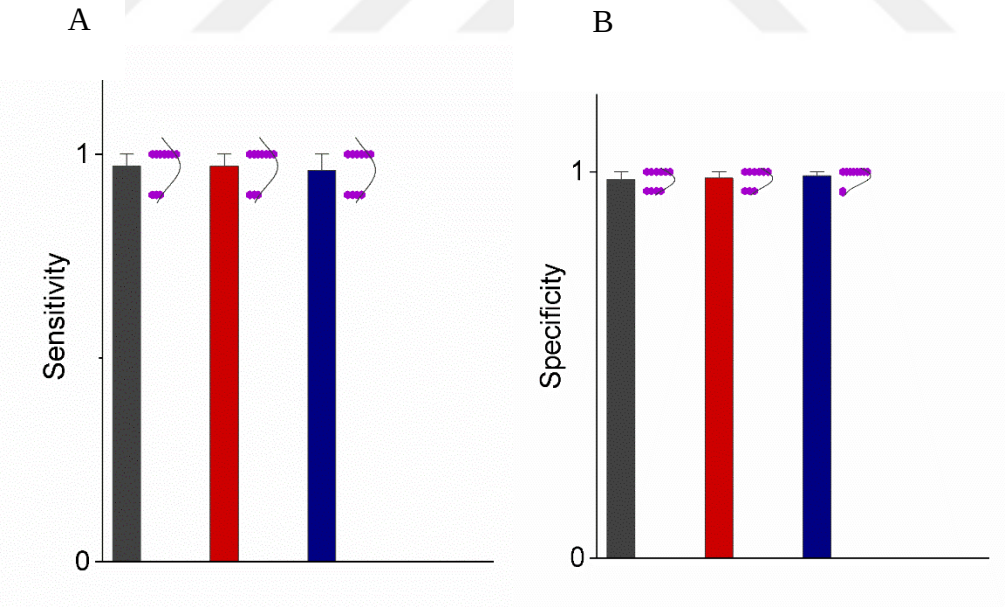

Figure 4.3: (A) The sensitivity calculation plot based on the three pressure patterns applied. (B) The specificity calculation plot based on the three pressure patterns applied.

4.2 Temperature sensor experiment

The temperature experiment comprises three distinct applied temperature patterns (~40 ˚C) to the sensor using a heat gun. Initially, a minor temperature stimulation is administered, succeeded by a substantial stimulation endured for an extended duration. Subsequently, another minor temperature stimulation is employed (Figure 4.4A). The alteration in capacitance, observed as a reaction to the external applied temperature, represents the sensor's output. The output of the sensor shows a good resemblance to the applied temperature pattern. Thermo-haptic feedback is also a crucial function to provide users with a more comprehensive perception of the object. The temperature actuator responds to the temperature applied to the sensor. A voltage signal is given to the actuator in the form of a pulse when the change in capacitance occurs.

The placement of a temperature actuator on the human wrist and its activation in response to the sensor's output constitute the methodology. The participants were asked to differentiate between the applied patterns of temperature and the response was recorded in the form of a questionnaire. The ensuing responses were documented through a questionnaire. Statistical analysis was performed through a confusion matrix, depicted in Figure 4.4B, displaying a 91.7 % accuracy rate.

To establish a comparison, the actuator was also positioned on a participant's finger and wrist, enabling discrimination of applied temperatures on distinct body locations. Thermal camera images portray the actuator temperature on both the human wrist and finger, demonstrating uniform temperature (Figure 4.5). The applied temperature can be controlled by the voltage signal from the electronics based on the applied temperature to the sensor, enabling us to differentiate objects with different thermal properties, e.g., differentiating different objects based on their surface thermal state, etc.

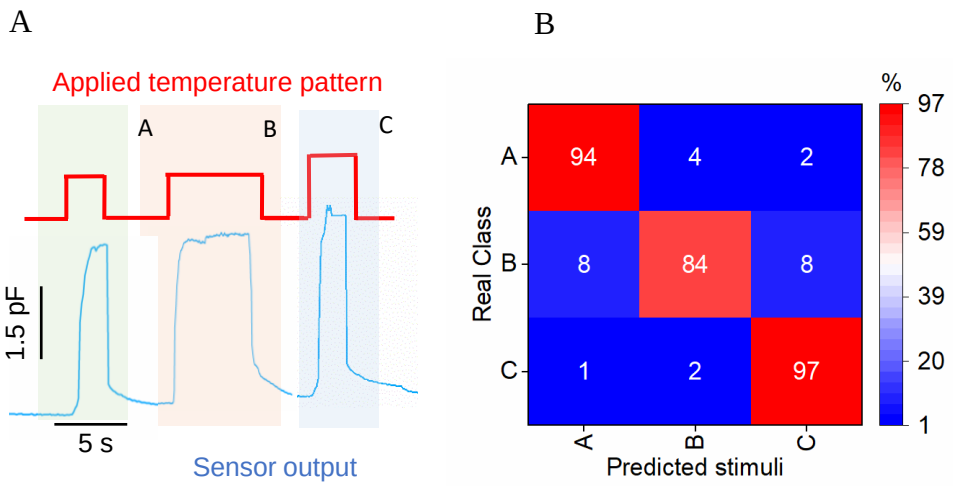

Figure 4.4: (A) Picture of the applied temperature pattern and the output of the sensor. (B) The performance obtained during the temperature experiment is in the form of a confusion matrix.

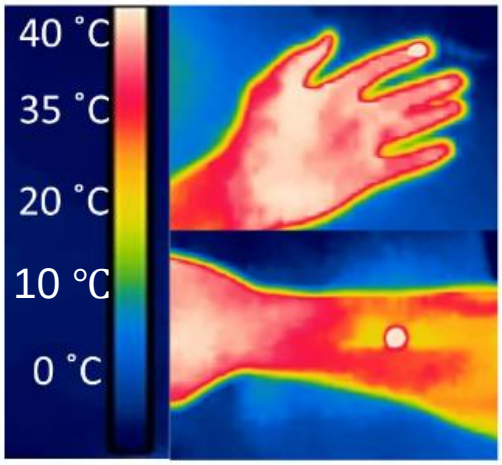

Figure 4.5: Thermal images of the actuator applied to the finger and wrist of the human subject.

4.3 Vibration sensor experiment

A tactile feedback system of the vibration sensation is realized by integrating the vibration sensor output into the vibration actuator. The Vibration sensation from the sensor's output was translated to the vibration actuator (coin cell motor) via electronic circuitry. The frequency of the waveform was calculated by taking the real-time FFT which gives the dominant frequency. The vibration motor (Actuator) vibrated with the output dominant frequency generated by the sensor. Figure 4.6A illustrates the vibration pattern applied to the sensor with one vibration at 75 Hz followed by vibrating twice at the same frequency and then three times vibration. The output vibration frequency of the sensor can be observed which shows the three frequencies signals produced in response to the applied vibration patterns. The quantitative results of the experiment were realized in the form of statistical analysis. The confusion matrix illustrates the overall performance of this task with 98% correct answers (Figure 4.6B). Moreover, the confusion matrix was utilized to compute sensitivity and specificity values, revealing a notable level of sensitivity (SE = 0.98) and specificity (SP = 0.99) (Figure 4.7 A and B). The findings demonstrate the system's ability to deliver vibrations to individuals with upper limb amputation at various frequencies.

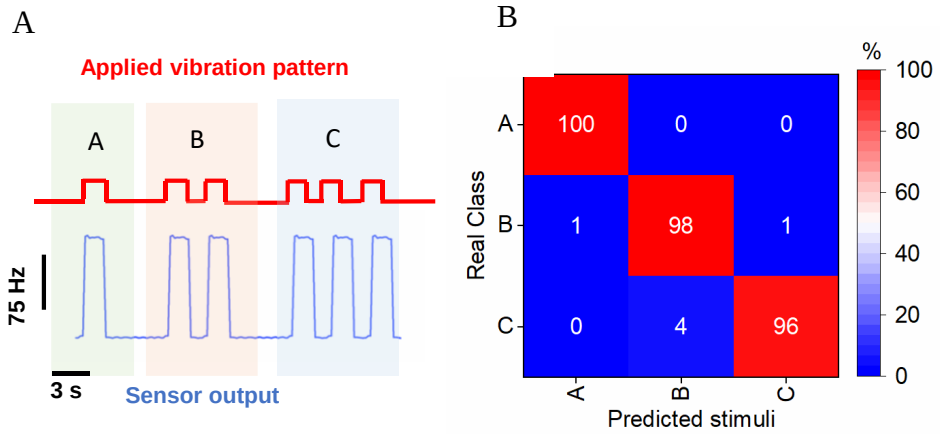

Figure 4.6: Picture of the applied vibration pattern and the output frequency (75 Hz) response of the sensor. (B) Confusion matrix of the response obtained from the vibration experiment.

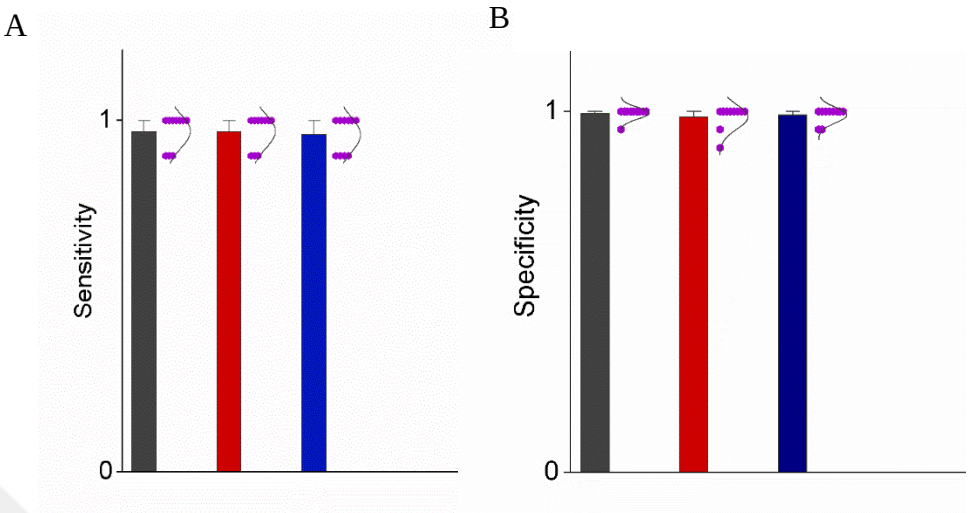

Figure 4.7: (A) The sensitivity calculation plot based on the three vibration patterns applied. (B) The specificity calculation plot based on the three vibration patterns applied.

4.4 Texture sensor experiment

The recognition of tactile textures is an intricate procedure that involves the spatial encoding of the coarse texture's geometric properties and the vibrotactile encoding of the fine textures. We mimicked this mechanism by utilizing a system that integrates the fabricated piezoelectric-based texture sensors with the coin cell vibration motors as a texture actuator. We chose three surfaces of varying roughness: the initial surface featured ridges roughly measuring 1.1 mm, the second surface displayed a roughness of approximately 0.8 mm, and the third surface exhibited a roughness of approximately 0.44 mm. The rough surface was placed on a moving stage (LTS150, Thorlabs Inc.) with a controlled speed (2 mm/s in this experiment), and the sensor on the glove was placed on a fixed stage to interact with the moving stage. Figure 4.8A shows the applied pattern of surfaces having the roughness mentioned above and the sensor’s output frequency calculated by taking the real-time FFT in the microcontroller.

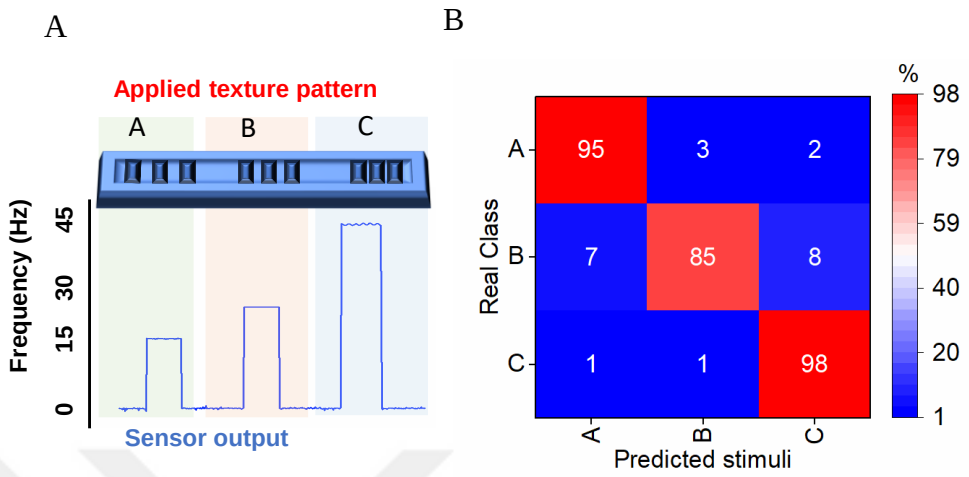

Figure 4.8:(A) Picture of the applied texture surfaces to the sensor and the out frequencies of the sensor. (B) Overall performance of the texture sensor and feedback in the form of a confusion matrix.

Two coin-cell vibration motors were used as an actuator, and the vibration frequency produced by the sensors was given to the motors to vibrate. There was a certain delay between the actuation time of the motors which corresponded to the roughness of the surface. Experimental trials were performed, and participants were asked to differentiate between the three surfaces. Statistical analysis results were shown in the form of a confusion matrix which shows 92.7 % accurate answers (Figure 4.8B). Furthermore, sensitivity and specificity values of SE = 0.89 and SP = 0.96 are calculated from the confusion matrix (Figure 4.9 A and B).

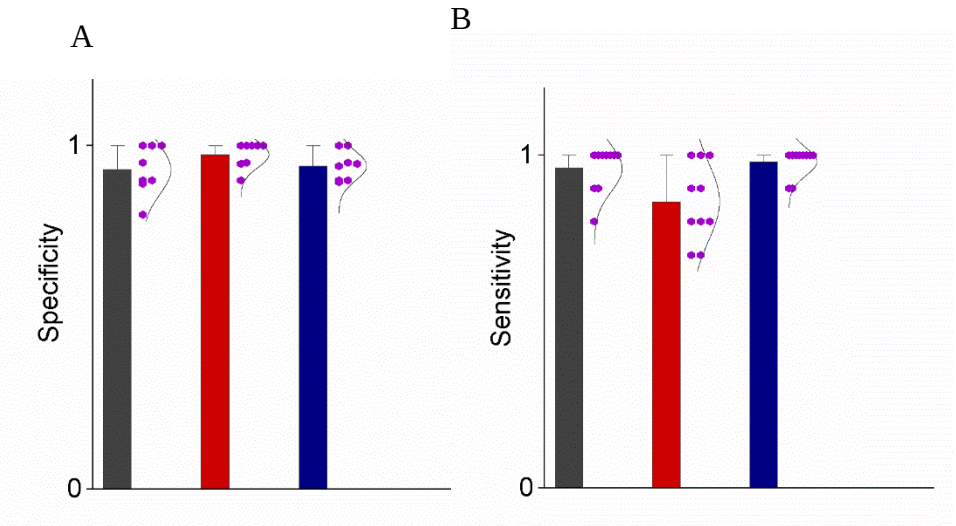

Figure 4.9: (A) The sensitivity calculation plot based on the three texture patterns applied. (B) The specificity calculation plot based on the three texture patterns applied.

Chapter 5:

MATERIALS AND METHODS

5.1 Fabrication of the miniaturized array of sensor

A standard six-inch silicon wafer (Siegert Wafer Inc.) was diced into 2.5 cm × 2.5 cm small chips using a dicing saw (DAD 3221, DISCO Inc.). These silicon chips served as temporary substrates for the fabrication process. The diced chip was sequentially submerged in acetone and isopropyl alcohol (IPA), each time undergoing a 5-minute ultrasonic bath for cleaning. Following, the chip was blow-dried with N2 and treated with oxygen-plasma (SI 500, Sentech Instruments Inc.) for 60 seconds. Subsequently, the chip was spin-coated with polyimide (PI) (Sigma Aldrich Inc.) and baked at 100 °C for 1 hour, followed by baking at 300 °C for 1 hour. Then, aluminum was sputtered to a thickness of 120 nm, followed by the sputtering of 30 nm of chromium onto the aluminum layer (PVD 75 PRO-Line, Kurt J. Lesker Inc.). Subsequently, a solution of 15 wt% Poly(vinylidenefluoride-co-trifluoroethylene) (PVDF-TrFE) (FC20, Piezotech Inc.) was prepared by mixing PVDF-TrFE powder in dimethylformamide (DMF). The mixture was stirred on a temperature-controlled magnetic stirrer for 3 hours at 80°C and then filtered through a 0.45 μm PTFE membrane. Before applying the PVDF-TrFE layer, Kapton tape was used to cover a small portion of the sputtered metal to ensure a connection with the bottom electrode after fabrication. The PVDF-TrFE solution was first spin coated and baked at 140°C for 5 minutes, followed by a second spin coating and baking at the same temperature for 20 minutes. AZ5214 positive photoresist (AZ5214, MicroChemicals Inc.) was spin-coated and soft-baked at 110°C for 55 seconds before patterns were defined with UV photolithography (μMLA 100, Heidelberg Instruments Inc.). AZ 726 MIF developer (AZ 726 MIF, MicroChemicals Inc.) was applied for 110 seconds for the development. In order to remove excess photoresist from the developed regions, 60 s of oxygen-plasma treatment (SI 500, Sentech Instruments Inc.) was applied. For the top electrode, a 30 nm chromium layer and a 120 nm aluminum layer were sputtered (PVD 75 PRO-Line, Kurt J. Lesker Inc.). Lift-off was performed using methanol to avoid damaging the PVDF-TrFE film. To enhance the piezoelectric properties of the PVDF-TrFE film, polarization

was conducted using DC voltage. The voltage gradually increased from 20 V to a final value of 300 V, and the 300 V field was applied for 30 minutes.

Chapter 6:

CONCLUSION

In this study, we introduce a piezoelectric-based electronic skin capable of multisensory tactile sensation of the temperature, ressure, Vibration, and texture located at the interface between the prosthetic hand and the soft skin of the residual limb. Demonstration of the multifunctional e-skin on different participants without any irritation and thermal or mechanical perturbation of the skin surface illustrates its robust capabilities in the prosthesis. By restoring the sensory feedback mechanism of the prosthesis, this near-natural system significantly enhances the quality of life for individuals with upper limb amputation. Our miniaturized design of the e-skin also contains a sensory feedback system that enables the correct sensory motor integration between the central nervous system of the user and the artificial limb. We tested the real-time implementation of the e-skin system by placing the miniaturized array of sensors on the glove which mimicked an upper limb prosthetic. The real-time feedback mechanism was achieved by using a series of actuators assembled with a miniaturized electronic circuit design attached to the soft skin. The capabilities rely critically on three main advances over the technologies reported previously: (i) multifunctional miniaturized design of e-skin system, (ii) miniaturized design of the electronic circuitry for signal processing, and (iii) the feedback mechanism achieved by using actuators. Compared with the reported e-skins with different working mechanisms, this piezoelectric-capacitive e-skin system is a complete package in terms of the number of comprehensive sensations, linearity, and miniaturized size of an array (Table S1). Moreover, compared

to different e-skins reported, the reported e-skin has some advantages: the miniaturized sensing array possesses four comprehensive sensations with a haptic feedback mechanism, and the sensors exhibit a wide range of sensations which makes the e-skin system to cover the limit of the natural sensation of the human skin (Table S2). type of multifunctional tactile sensing system creates a promising route for scalable manufacturing of the e-skins, which is highly desired in applications like prosthetics (Yang et al., 2019; H. Zhao et al., 2016) and surgeon robots (Wei et al., 2022; J. Zhu et al., 2021).

The miniaturized sensors and electronics strategies hold significant potential, particularly for individuals utilizing wearable robots in rehabilitation. Benchtop studies and practical implementation of the system on an upper limb prosthesis demonstrate the usability of all the critical functional aspects and its adaptability for other types of limb amputations. Future work could focus on establishing wireless connections between the sensors and actuators and integrating an internal power source to eliminate the need for an external power supply. Moreover, optimizing the e-skin system design for other amputations could enhance its versatility.

Table 1: Comparison of the e-skins with different working mechanisms.

Working mechanism	***Linearity***	***Number of sensations***	***Haptic feedback***	***Size of array***	***Standalone electronics***	***Reference***
Electromagnetic induction	R2= 0.994	1	YES	12 mm (1 array)	YES	*(7)*
Resistive	R2= 0.99	2	NO	3 X 1.8 cm	YES	*(12)*
Piezoresistive	NA	3	NO	10 mm (1 array)	NO	*(30)*
piezoelectric, triboelectric, piezoresistive	NA	2	NO	30 x 30 mm	NO	*(34)*
Piezoelectric-capacitive	NA	4	NO	13 mm (2 arrays)	NO	*(38)*
Piezo-thermic, capacitive, thermistors	NA	4	YES	13.9 x 10 cm	NO	*(39)*
Capacitive	NA	3	YES		YES	*(40)*
Piezoelectric-capacitive	R2= 0.991	4	YES	10 x 10 mm (2 arrays)	YES	Our work

Table 2: Comparison of the range of the e-skin sensors for the comprehensive sensations.

Pressure sensing range	***Temperature sensing range***	***Vibration sensing range***	***Texture sensing range***	***Reference***
NA	NA	70-740 Hz	NA	*(6)*
0-400 kPa	23-35 ℃	NA	NA	*(12)*
0-80 kPa	22-60 ℃	NA	NA	*(23)*
0-25 kPa	22-70 ℃	NA	NA	*(24)*
NA	NA	NA	21-56 Hz	*(45)*
0-10 kPa	22-60 ℃	35-100 Hz	2.5-45 Hz	Our work

BIBLIOGRAPHY

Bae, G. Y., Han, J. T., Lee, G., Lee, S., Kim, S. W., Park, S., Kwon, J., Jung, S., & Cho, K. (2018). Pressure/temperature sensing bimodal electronic skin with stimulus discriminability and linear sensitivity. *Advanced Materials*, *30*(43), 1803388.

Bensmaïa, S. J., & Hollins, M. (2003). The vibrations of texture. *Somatosensory & Motor Research*, *20*(1), 33–43.

Boutry, C. M., Negre, M., Jorda, M., Vardoulis, O., Chortos, A., Khatib, O., & Bao, Z. (2018). A hierarchically patterned, bioinspired e-skin able to detect the direction of applied pressure for robotics. *Science Robotics*, *3*(24). doi: 10.1126/SCIROBOTICS.AAU6914/SUPPL_FILE/AAU6914_SM.PDF

Cai, M., Jiao, Z., Nie, S., Wang, C., Zou, J., & Song, J. (2021). A multifunctional electronic skin based on patterned metal films for tactile sensing with a broad linear response range. *Science Advances*, *7*(52), eabl8313.

Chen, H., Miao, L., Su, Z., Song, Y., Han, M., Chen, X., Cheng, X., Chen, D., & Zhang, H. (2017). Fingertip-inspired electronic skin based on triboelectric sliding sensing and porous piezoresistive pressure detection. *Nano Energy*, *40*, 65–72.

Chen, S., Chen, Y., Yang, J., Han, T., & Yao, S. (2023). Skin-integrated stretchable actuators toward skin-compatible haptic feedback and closed-loop human-machine interactions. *Npj Flexible Electronics 2023 7:1*, *7*(1), 1–12. doi: 10.1038/s41528-022-00235-y

Chen, Y., Lei, H., Gao, Z., Liu, J., Zhang, F., Wen, Z., & Sun, X. (2022). Energy autonomous electronic skin with direct temperature-pressure perception. *Nano Energy*, *98*, 107273.

Cho, S., Jang, S., Lee, D., Ra, Y., Kam, D., Kim, J. W., Shin, D., Seo, K. D., & Choi, D. (2022). Self-powered hybrid triboelectric–piezoelectric electronic skin based on P (VDF-TrFE) electrospun nanofibers for artificial sensory system. *Functional Composites and Structures*, *4*(4), 045005.

Chortos, A., Liu, J., & Bao, Z. (2016). Pursuing prosthetic electronic skin. *Nature Materials*, *15*(9), 937–950.

Chun, S., Hong, A., Choi, Y., Ha, C., & Park, W. (2016). A tactile sensor using a conductive graphene-sponge composite. *Nanoscale*, *8*(17), 9185–9192.

Dai, Y., & Gao, S. (2021). A flexible multi-functional smart skin for force, touch position, proximity, and humidity sensing for humanoid robots. *IEEE Sensors Journal*, *21*(23), 26355–26363.

D'Anna, E., Valle, G., Mazzoni, A., Strauss, I., Iberite, F., Patton, J., Petrini, F. M., Raspopovic, S., Granata, G., & Di Iorio, R. (2019). A closed-loop hand prosthesis with simultaneous intraneural tactile and position feedback. *Science Robotics*, *4*(27), eaau8892.

Farina, D., & Aszmann, O. (2014). Bionic limbs: clinical reality and academic promises. *Science Translational Medicine*, *6*(257), 257ps12-257ps12.

Fastier-Wooller, J. W., Dinh, T., Tran, C.-D., & Dao, D. V. (2021). Pressure and temperature sensitive e-skin for in situ robotic applications. *Materials & Design*, *208*, 109886.

Jones, L. A., & Lederman, S. J. (2006). *Human hand function*. Oxford university press.

Jung, Y. H., Yoo, J.-Y., Vázquez-Guardado, A., Kim, J.-H., Kim, J.-T., Luan, H., Park, M., Lim, J., Shin, H.-S., & Su, C.-J. (2022a). A wireless haptic interface for programmable patterns of touch across large areas of the skin. *Nature Electronics*, *5*(6), 374–385.

Jung, Y. H., Yoo, J.-Y., Vázquez-Guardado, A., Kim, J.-H., Kim, J.-T., Luan, H., Park, M., Lim, J., Shin, H.-S., & Su, C.-J. (2022b). A wireless haptic interface for programmable patterns of touch across large areas of the skin. *Nature Electronics*, *5*(6), 374–385.

Kwak, J. W., Han, M., Xie, Z., Chung, H. U., Lee, J. Y., Avila, R., Yohay, J., Chen, X., Liang, C., Patel, M., Jung, I., Kim, J., Namkoong, M., Kwon, K., Guo, X., Ogle, C., Grande, D., Ryu, D., Kim, D. H., … Rogers, J. A. (2020). Wireless sensors for continuous, multimodal measurements at the skin interface with lower limb prostheses. *Science Translational Medicine*, *12*(574), 4327. doi: 10.1126/SCITRANSLMED.ABC4327/SUPPL_FILE/ABC4327_SM.PDF

Lee, G., Son, J. H., Lee, S., Kim, S. W., Kim, D., Nguyen, N. N., Lee, S. G., & Cho, K. (2021). Fingerpad-inspired multimodal electronic skin for material discrimination and texture recognition. *Advanced Science*, *8*(9), 2002606.

Li, D., He, J., Song, Z., Yao, K., Wu, M., Fu, H., Liu, Y., Gao, Z., Zhou, J., Wei, L., Zhang, Z., Dai, Y., Xie, Z., & Yu, X. (2021). Miniaturization of mechanical

actuators in skin-integrated electronics for haptic interfaces. *Microsystems & Nanoengineering 2021 7:1*, *7*(1), 1–9. doi: 10.1038/s41378-021-00301-x

Li, D., Zhou, J., Yao, K., Liu, S., He, J., Su, J., Qu, Q., Gao, Y., Song, Z., Yiu, C., Sha, C., Sun, Z., Zhang, B., Li, J., Huang, L., Xu, C., Wong, T. H., Huang, X., Li, J., … Yu, X. (2022). Touch IoT enabled by wireless self-sensing and haptic-reproducing electronic skin. *Science Advances*, *8*(51). doi: 10.1126/SCIADV.ADE2450/SUPPL_FILE/SCIADV.ADE2450_MOVIES_S1_TO_S6.ZIP

Li, G., Liu, S., Mao, Q., & Zhu, R. (2022). Multifunctional electronic skins enable robots to safely and dexterously interact with human. *Advanced Science*, *9*(11), 2104969.

Li, P., Anwar Ali, H. P., Cheng, W., Yang, J., & Tee, B. C. K. (2020). Bioinspired prosthetic interfaces. *Advanced Materials Technologies*, *5*(3), 1900856.

Li, Q., Zhang, L., Tao, X., & Ding, X. (2017). Review of flexible temperature sensing networks for wearable physiological monitoring. *Advanced Healthcare Materials*, *6*(12), 1601371.

Liang, Z., Cheng, J., Zhao, Q., Zhao, X., Han, Z., Chen, Y., Ma, Y., & Feng, X. (2019). High-performance flexible tactile sensor enabling intelligent haptic perception for a soft prosthetic hand. *Advanced Materials Technologies*, *4*(8), 1900317.

Liu, F., Deswal, S., Christou, A., Baghini, M. S., Chirila, R., Shakthivel, D., Chakraborty, M., & Dahiya, R. (2022). Printed synaptic transistor-based electronic skin for robots to feel and learn. *Science Robotics*, *7*(67), 7286. doi: 10.1126/SCIROBOTICS.ABL7286/SUPPL_FILE/SCIROBOTICS.ABL7286_MOVIES_S1_TO_S5.ZIP

Liu, Y., Yiu, C., Song, Z., Huang, Y., Yao, K., Wong, T., Zhou, J., Zhao, L., Huang, X., Nejad, S. K., Wu, M., Li, D., He, J., Guo, X., Yu, J., Feng, X., Xie, Z., & Yu, X. (2022). Electronic skin as wireless human-machine interfaces for robotic VR. *Science Advances*, *8*(2), 6700. doi: 10.1126/SCIADV.ABL6700/SUPPL_FILE/SCIADV.ABL6700_MOVIES_S1_TO_S7.ZIP

Pan, L., Chortos, A., Yu, G., Wang, Y., Isaacson, S., Allen, R., Shi, Y., Dauskardt, R., & Bao, Z. (2014). An ultra-sensitive resistive pressure sensor based on hollow-

sphere microstructure induced elasticity in conducting polymer film. *Nature Communications*, *5*(1), 3002.

Pang, Y., Xu, X., Chen, S., Fang, Y., Shi, X., Deng, Y., Wang, Z.-L., & Cao, C. (2022). Skin-inspired textile-based tactile sensors enable multifunctional sensing of wearables and soft robots. *Nano Energy*, *96*, 107137.

Petrini, F. M., Valle, G., Bumbasirevic, M., Barberi, F., Bortolotti, D., Cvancara, P., Hiairrassary, A., Mijovic, P., Sverrisson, A. Ö., Pedrocchi, A., Divoux, J. L., Popovic, I., Lechler, K., Mijovic, B., Guiraud, D., Stieglitz, T., Alexandersson, A., Micera, S., Lesic, A., & Raspopovic, S. (2019). Enhancing functional abilities and cognitive integration of the lower limb prosthesis. *Science Translational Medicine*, *11*(512). doi: 10.1126/SCITRANSLMED.AAV8939/SUPPL_FILE/AAV8939_SM.PDF

Qiu, Y., Tian, Y., Sun, S., Hu, J., Wang, Y., Zhang, Z., Liu, A., Cheng, H., Gao, W., & Zhang, W. (2020). Bioinspired, multifunctional dual-mode pressure sensors as electronic skin for decoding complex loading processes and human motions. *Nano Energy*, *78*, 105337.

Raichle, K. A., Hanley, M. A., Molton, I., Kadel, N. J., Campbell, K., Phelps, E., Ehde, D., & Smith, D. G. (2008). Prosthesis use in persons with lower-and upper-limb amputation. *Journal of Rehabilitation Research and Development*, *45*(7), 961.

Rostamian, B., Koolani, M., Abdollahzade, P., Lankarany, M., Falotico, E., Amiri, M., & V. Thakor, N. (2022). Texture recognition based on multi-sensory integration of proprioceptive and tactile signals. *Scientific Reports*, *12*(1), 21690.

Shih, B., Shah, D., Li, J., Thuruthel, T. G., Park, Y. L., Iida, F., Bao, Z., Kramer-Bottiglio, R., & Tolley, M. T. (2020). Electronic skins and machine learning for intelligent soft robots. *Science Robotics*, *5*(41), 9239. doi: 10.1126/SCIROBOTICS.AAZ9239/ASSET/FB86D6D2-9D34-4AC2-9F75-D62000F8F7EE/ASSETS/GRAPHIC/AAZ9239-F6.JPEG

Sotgiu, E., Aguiam, D. E., Calaza, C., Rodrigues, J., Fernandes, J., Pires, B., Moreira, E. E., Alves, F., Fonseca, H., & Dias, R. (2020). Surface texture detection with a new sub-mm resolution flexible tactile capacitive sensor array for multimodal artificial finger. *Journal of Microelectromechanical Systems*, *29*(5), 629–636.

Thuruthel, T. G., Shih, B., Laschi, C., & Tolley, M. T. (2019). Soft robot perception using embedded soft sensors and recurrent neural networks. *Science Robotics*,

4(26), 1488. doi: 10.1126/SCIROBOTICS.AAV1488/SUPPL_FILE/AAV1488_SM.PDF

Vicentini, M., & Botturi, D. (2010). Perceptual issues improve haptic systems performance. *Advances in Haptics*, 415–438.

Wang, Y., Wu, H., Xu, L., Zhang, H., Yang, Y., & Wang, Z. L. (2020). Hierarchically patterned self-powered sensors for multifunctional tactile sensing. *Science Advances*, *6*(34), eabb9083.

Wei, D., Guo, J., Qiu, Y., Liu, S., Mao, J., Liu, Y., Chen, Z., Wu, H., & Yin, Z. (2022). Monitoring the delicate operations of surgical robots via ultra-sensitive ionic electronic skin. *National Science Review*, *9*(12), nwac227.

Xiong, W., Feng, H., Liwang, H., Li, D., Yao, W., Duolikun, D., Zhou, Y., & Huang, Y. (2022). Multifunctional tactile feedbacks towards compliant robot manipulations via 3D-shaped electronic skin. *IEEE Sensors Journal*, *22*(9), 9046–9056.

Yang, J. C., Mun, J., Kwon, S. Y., Park, S., Bao, Z., & Park, S. (2019). Electronic skin: recent progress and future prospects for skin-attachable devices for health monitoring, robotics, and prosthetics. *Advanced Materials*, *31*(48), 1904765.

Yao, G., Xu, L., Cheng, X., Li, Y., Huang, X., Guo, W., Liu, S., Wang, Z. L., & Wu, H. (2020). Bioinspired triboelectric nanogenerators as self-powered electronic skin for robotic tactile sensing. *Advanced Functional Materials*, *30*(6), 1907312.

Yin, J., Hinchet, R., Shea, H., & Majidi, C. (2021). Wearable soft technologies for haptic sensing and feedback. *Advanced Functional Materials*, *31*(39), 2007428.

Yu, Y., Nassar, J., Xu, C., Min, J., Yang, Y., Dai, A., Doshi, R., Huang, A., Song, Y., Gehlhar, R., Ames, A. D., & Gao, W. (2020). Biofuel-powered soft electronic skin with multiplexed and wireless sensing for human-machine interfaces. *Science Robotics*, *5*(41). doi: 10.1126/SCIROBOTICS.AAZ7946/SUPPL_FILE/AAZ7946_SM.PDF

Zang, Y., Zhang, F., Di, C., & Zhu, D. (2015). Advances of flexible pressure sensors toward artificial intelligence and health care applications. *Materials Horizons*, *2*(2), 140–156.

Zhao, H., O'brien, K., Li, S., & Shepherd, R. F. (2016). Optoelectronically innervated soft prosthetic hand via stretchable optical waveguides. *Science Robotics*, *1*(1), eaai7529.

Zhao, S., & Zhu, R. (2017). Electronic skin with multifunction sensors based on thermosensation. *Advanced Materials*, *29*(15), 1606151.

Zhu, J., Lyu, L., Xu, Y., Liang, H., Zhang, X., Ding, H., & Wu, Z. (2021). Intelligent soft surgical robots for next-generation minimally invasive surgery. *Advanced Intelligent Systems*, *3*(5), 2100011.

Zhu, M., Sun, Z., Zhang, Z., Shi, Q., He, T., Liu, H., Chen, T., & Lee, C. (2020). Haptic-feedback smart glove as a creative human-machine interface (HMI) for virtual/augmented reality applications. *Science Advances*, *6*(19). doi: 10.1126/SCIADV.AAZ8693/SUPPL_FILE/AAZ8693_SM.PDF

Zhu, P., Wang, Y., Wang, Y., Mao, H., Zhang, Q., & Deng, Y. (2020). Flexible 3D architectured piezo/thermoelectric bimodal tactile sensor array for E-skin application. *Advanced Energy Materials*, *10*(39), 2001945.

Ziegler-Graham, K., MacKenzie, E. J., Ephraim, P. L., Travison, T. G., & Brookmeyer, R. (2008). Estimating the Prevalence of Limb Loss in the United States: 2005 to 2050. *Archives of Physical Medicine and Rehabilitation*, *89*(3), 422–429. doi: 10.1016/J.APMR.2007.11.005